SELF-STRUCTURING HEAD-WORN ANTENNA

By

Korede Akinlabi-Oladimeji

A THESIS

Submitted to
Michigan State University
in partial fulfillment of the requirements
for the degree of

MASTER OF SCIENCE

Electrical Engineering

2012

ABSTRACT

SELF-STRUCTURING HEAD-WORN ANTENNA

By

Korede Akinlabi-Oladimeji

A wearable patch antenna is investigated in this thesis. In particular, a patch antenna that can be borne on a human head is investigated by assessing its performance in free space and in proximity to a human head. The antenna is a self-structuring patch antenna placed conformal with a curved surface. An integral part of the antenna system is a set of switches connected from the patch surface to the ground plane. Changes in the electrical shape of the antenna can be achieved by changing the switch configurations. This allows for effective use of the antenna even in the vicinity of the human body despite the resulting coupling effects.

Simulations were carried out on the antenna in free space between 1 GHz and 2 GHz. Furthermore, simulations were run with the antenna in proximity to a human head model over the same frequency range. A genetic algorithm is used to search effectively through the large number of switch states for antenna configurations with desirable performance.

Measurements that were carried out on a fabricated prototype antenna are presented. Experiments were performed with the antenna in free space. Random search measurements were undertaken to gain a general sense of the impedance distribution of the antenna states. Finally, targeted genetic-algorithm based optimizations were carried out at specific frequencies.

For my father, Akinlabi Oladimeji.

ACKNOWLEDGMENTS

- Dr Edward Rothwell
- Dr Percy Pierre
- Dr Ross
- Raenita Fenner
- Dr Folake Oladimeji

Table of Contents

List of Tables . . . . . **vi**

List of Figures . . . . . **ix**

1 Introduction **1**
1.1 Wearable Antennas 1
1.2 Self-Structuring Antennas 2

2 Simulations **5**
2.1 Genetic Algorithms 5
2.2 Antenna Model 6
2.3 Human head model 7
2.4 Biological Tissue Modeling 8
2.4.1 Dielectric Spectrum of Tissue 8
2.4.2 Responses of Real Systems – Conduction & Multiple Relaxations . . 9
2.4.3 Multiple Relaxation Models – Distribution of Relaxation Times . . . 10
2.5 Free-space Optimization 12
2.5.1 Antenna & Head Simulations 14

3 Measurements **42**
3.1 Antenna Prototype Fabrication 42
3.2 Free Space Measurements 44
3.2.1 Random Search Measurements 44
3.2.2 Single frequnecy Optimization 44
3.2.3 Pattern Measurements 45

4 Conclusions & Future Work **77**

Bibliography **79**

List of Tables

2.1 Select permittivity values over the frequency range considered. 20

2.2 Results from free space simulations of head worn antenna 21

3.1 Random Search vs. GA 70

List of Figures

1.1 Self-structuring antenna system 4

2.1 The head-worn antenna pin layout. For interpretation of the references to color in this and all other figures the reader is referred to the electronic version of this thesis. 15

2.2 Antenna ground plane alone. 16

2.3 Head-worn patch antenna desinged in FEKO 17

2.4 Head model in used in FEKO simulations 18

2.5 Minimum VSWR values obtained for simulated head-worn antenna found using GA search. 19

2.6 Reflection Coefficient of head-worn antenna with all switches open 22

2.7 Reflection coefficient of head-worn antenna at 1.0 GHz 23

2.8 Reflection coefficient of head-worn antenna at 1.1 GHz 24

2.9 Reflection coefficient of head-worn antenna at 1.2 GHz 25

2.10 Reflection coefficient of head-worn antenna at 1.3 GHz 26

2.11 Reflection coefficient of head-worn antenna at 1.4 GHz 27

2.12 Reflection coefficient of head-worn antenna at 1.5 GHz 28

2.13 Reflection coefficient of head-worn antenna at 1.6 GHz 29

2.14 Reflection coefficient of head-worn antenna at 1.8 GHz 30

2.15 Reflection coefficient of head-worn antenna at 1.9 GHz 31

2.16 Reflection coefficient of head-worn antenna at 1.0 GHz 32

2.17 Reflection coefficient of head-worn antenna at 1.5 GHz – multiple frequencies 33

2.18 Rank comparison at 1.1 GHz 34

2.19 Rank comparison at 1.3 GHz 35

2.20 Rank comparison at 1.4 GHz 36
2.21 Pattern of best state at 1.1 GHz – Azimuthal plane 37
2.22 Pattern of best state at 1.3 GHz – Azimuthal plane 38
2.23 Figure illustrating pattern plane measurement designations 39
2.24 Head and antenna with all the switches open 40
2.25 Head and antenna at 1.0 GHz 41

3.1 Picture of Prototype II 47
3.2 Picture of Prototype II 48
3.3 Head-worn antenna switch layout 49
3.4 Reflection coefficient of antenna with all the switches open 50
3.5 Illustration of experimental setup 51
3.6 Switch close-up 52
3.7 Impedances of 100,000 random states at 100 MHz 53
3.8 Impedances of 100,000 random states at 200 MHz 54
3.9 Impedances of 100,000 random states at 300 MHz 55
3.10 Impedances of 100,000 random states at 400 MHz 56
3.11 Impedances of 100,000 random states at 500 MHz 57
3.12 Impedances of 100,000 random states at 600 MHz 58
3.13 Impedances of 100,000 random states at 700 MHz 59
3.14 Impedances of 100,000 random states at 800 MHz 60
3.15 Impedances of 100,000 random states at 900 MHz 61
3.16 Impedances of 100,000 random states at 1 GHz 62
3.17 Impedances of 100,000 random states at 1.1 GHz 63
3.18 Random Search Measurements 64

3.19 Random Search Measurements – minimum VSWR 65

3.20 Magnitude of the reflection coefficient for head-worn antenna optimized at 160 MHz 66

3.21 Magnitude of the reflection coefficient for head-worn antenna optimized at 280 MHz 67

3.22 Magnitude of the reflection coefficient for head-worn antenna optimized at 320 MHz 68

3.23 Magnitude of the reflection coefficient for head-worn antenna optimized at 200 MHz 69

3.24 Pattern of best state at 200 MHz – Azimuthal plane 71

3.25 Pattern of best state at 200 MHz – Elevation plane 72

3.26 Pattern of best state at 280 MHz – Azimuthal plane 73

3.27 Pattern of best state at 280 MHz – Elevation plane 74

3.28 Pattern of best state at 320 MHz – Azimuthal plane 75

3.29 Figure illustrating pattern plane measurement designation 76

Chapter 1

Introduction

1.1 Wearable Antennas

There has recently been considerable emphasis on the development of wearable antennas suitable for various medical and military applications. For example, a medical application being explored that requires wearable antennas is the use of body area networks for the real-time monitoring of the vital signs of an individual. The utility of such wearable antennas depends largely on their ability to meet desired performance specifications while in close proximity to a human wearer without posing a great radiation hazard to the wearer, since the deposition of large amounts of radiation into the human body is obviously undesirable.

Some work has been done in the design of wearable antennas by Wang [1], Lebaric et al. [2], and others. Wang has reported the design of a helmet antenna that meets regulatory requirements while providing good performance between 600 MHz and 4 GHz [1]. Lebaric has developed an omni-directional antenna integrated into military helmets that works over a frequency range of a decade [2]. In addition, implantable antennas have been investigated by researchers at UCLA [3]. The types of antennas that have been typically used in the building of wearable antennas are planar dipoles, monopoles and planar inverted-F antennas.

Presently, there are some issues that are holding back the development of wearable anten-

nas, namely the narrow-band nature of existing antennas and the need for better radiation safety. The self-structuring antenna is a class of antennas that has been investigated as a means of overcoming both of these issues. The self-structuring antenna is briefly discussed in the section that follows.

1.2 Self-Structuring Antennas

The underlying operating principle for the antenna considered in this thesis is that of the self-structuring antenna. The self-structuring antenna, invented at MSU in the year 2000 [4], is a class of antennas that adapts the electrical shape of an antenna to varying environmental conditions. A wide tunable bandwidth is the prevailing advantage of the self-structuring antenna that lends itself to application to the wearable antenna problem.

In its original conception, the self-structuring antenna is a template of wires interconnected by switches. Operation is through the selective opening and closing of the switches resulting in the antenna assuming different electrical shapes. In general, the self-structuring antenna comprises radiating elements (wires, patches, or slots) connected via switches.

Applications that have been proposed for the self-structuring antenna include wideband antennas, no-design antennas, mobile and wearable antennas [4]. The self-structuring antenna concept has been incorporated into the design of a patch antenna with a 2:1 bandwidth [5]. The work of this thesis is devoted to investigating the feasibility of designing a head-worn antenna that employs the self-structuring patch antenna concept.

The original self-structuring antenna system is shown in Figure 1.1. Optimization around some chosen performance criterion is achieved using a feedback signal from a receiver as shown in the figure. Alternatively, the feedback signal may be from a transmitter or some other sensor.

Since the number of possible antenna configurations for the self-structuring antenna is given by 2^N (where N is the number of switches), an efficient search algorithm is required to

find an optimal configuration. The use of different search routines such as genetic algorithms, simulated annealing and ant colony optimizations have been investigated [7].

It is believed that the advantages afforded by the application of the self-structuring antenna are three-fold: 1) the tunable nature of the antenna should make it able to withstand impedance changes due to dynamic interactions between the antenna and the wearer; 2) a constraint allowing for only states producing minimal radiation into the body can be imposed so as to meet appropriate regulatory requirements; and 3) inherent shielding characteristics because of the presence of a ground plane.

The chapters that follow detail simulations carried out to establish a proof of concept for the self-structuring head worn antenna, a description of the antenna fabrication process, and measurements carried out on a fabricated head worn antenna.

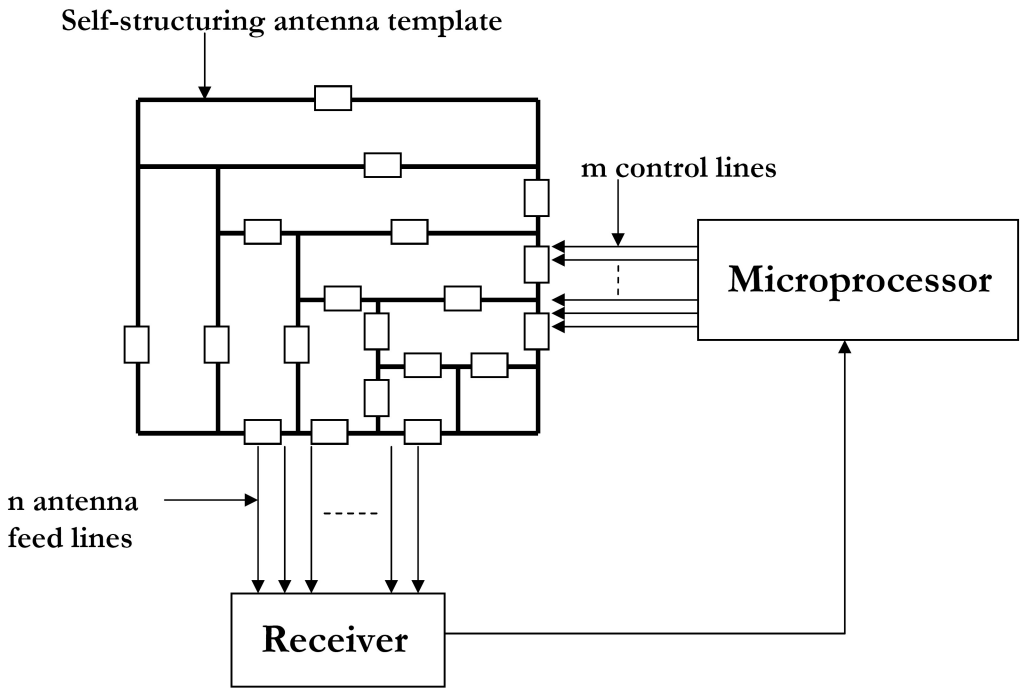

Figure 1.1: Self-structuring antenna system

Chapter 2

Simulations

Before embarking on the building of the antenna, simulations were carried out to establish a proof of concept for the proposed self-structuring head-worn antenna. The simulations detailed in this section were run with the analysis software FEKO [6], which employs the method of moments for solving electromagnetics problems.

As stated in the previous chapter, carrying out an exhaustive search of all possible antenna configurations would be a futile effort because of the large number of possible configurations. Hence, a genetic algorithm was utilized. A genetic algorithm was the chosen optimization method because it proved useful in previous work done with self-structuring antennas [7]. The genetic algorithm program that was used was developed by Dr John Ross and implanted in the program called GA-FEKO [8]. In the section that follows, genetic algorithms are briefly discussed.

2.1 Genetic Algorithms

Genetic algorithms are a class of algorithms inspired by the evolutionary processes in nature. They work by mimicking evolutionary processes such as inheritance, crossover and mutation. Typically, a genetic algorithm works on a given problem by going through the following steps:

1. Encoding of unknowns as chromosomes

2. Creation of an initial random population consisting of individual chromosomes

3. Computation of fitness values for each individual in the population

4. Creation of a new generation of individuals through the process of crossover

5. Imposition of diversity through the process of mutation

6. Carrying over of the fittest individuals to the next generation

7. Repetition of steps (2) through (6) until an acceptable solution is obtained

The crossover and mutation parameters are used to gain a balance between exploration of the search space and exploitation of results already obtained. Genetic algorithms find application in automotive design, the design of robots, telecommunications routing, scheduling, finance and investment strategies and so on. They are advantageous in situations where the search space is large and complex, domain knowledge is scarce, expert knowledge is difficult to encode or mathematical analysis is unavailable.

Genetic algorithms suffice for work with the self-structuring head-worn antenna since there is the lack of a search method based on mathematical analysis of the antenna. Also, the genetic algorithm lends itself to the binary nature of the problem since the on/off states of the switches can be directly encoded into the chromosomes as binary bits. Applications of genetic algorithms in electromagnetics are described in [9].

2.2 Antenna Model

Naturally, the proposed antenna had to be designed conformal to a human head. As such, the aim from the onset was to design a hemispherical patch antenna. The antenna is essentially a dielectric shell with a conforming patch on the top side and a ground plane underneath as shown in Figure 2.3. The dielectric shell supporting the antenna has an outer radius of

14 cm and a thickness of 1.5 mm. Shorting pins connect the patch to the ground plane and are controlled by switches to provide self-structuring behavior. To overcome difficulty that made use of inbuilt spherical design functionalities in FEKO inapplicable, surfaces that were used in actual simulations are polygonal rather than curved. Consequently, a more accurate model of the antenna is obtained with an increase in the number of sides of the polygons employed. An infinite sided polygon would correspond to a perfect description of the antenna.

It has been shown that better performance is obtained for the self-structuring antenna when the layout is set up in a way that the number of repeated antenna states is minimized [4]. As such, the layout is not drawn out in a symmetric fashion. The shorting pin layout used in the design of the head-worn antenna is shown in Figure 2.1. The designed ground plane is shown in Figure 2.2 with shorting pins protruding from it. These pins run from the ground plane through the substrate to the patch and are controlled by switches. The final resulting head worn antenna model is shown in Figure 2.3.

2.3 Human head model

The head model utilized is shown in Figure 2.4. The head is essentially a solid dielectric hemisphere connected to a truncated dielectric cone. The homogeneous average muscle model is utilized to describe its dielectric properties [20]. A full blown model including the corresponding constitutive parameter values for various parts of the head is not used because of the computational cost involved. The gain in model accuracy is not marked enough to justify the use of such a model [21]. Table 2.1 shows examples of the constitutive parameter values being dealt with over the frequency range considered.

2.4 Biological Tissue Modeling

Through the course of this work, salient points regarding the modeling of biological tissue were encountered and as such a minor discussion of work in this area is undertaken here. This is done to help with further work on body-worn self-structuring antennas since a proper characterization of human tissue that is in close proximity to these antennas is important in developing accurate models to study the behavior of such body-worn antennas.

Various methods have been explored to develop models for characterizing biological tissue in general and human tissue specifically. The leading models that have been used are the Debye model, the Cole-Cole model, the Cole-Davidson model and the Havriliak-Negami model. In particular, accurate prediction of experimental results has been demonstrated by Gabriel et al. [13]. Permittivity values used in this thesis for the simulations with the human head are obtained from the Cole-Cole model developed by Gabriel [13].

The great strides that have been made in dielectric models for human tissue mean that, if required, a more detailed model taking into consideration different permittivities of the different tissue in the head (bone, brain, skin e.t.c.) can also be utilized.

2.4.1 Dielectric Spectrum of Tissue

Application of a step electric field to a polar dielectric material results in the instantaneous establishment of electronic and atomic polarizations (instantaneous in comparison to the time scale of molecular orientation). The total polarization can be described by a first order process characterized by a time constant τ,

$$P = P_\infty + (P_s - P_\infty)[1 - \exp(-t/\tau)], \tag{2.1}$$

where P_s and P_∞ are the steady-state and instantaneous polarizations, respectively.

The complex relative permittivity for such a polar dielectric material may be obtained easily by performing a Laplace transform on the temporal expression of the permittivity to

obtain

$$\epsilon(\omega) = \epsilon^{'} - j\epsilon^{''} = \epsilon_{\infty} + \frac{(\epsilon_S - \epsilon_{\infty})}{1 + j\omega\tau}. \tag{2.2}$$

This expression is known as the Debye equation, where ϵ_S and ϵ_{∞} are the static and infinite permittivity, respectively, with ϵ_S being the permittivity at frequencies where $\omega\tau \ll 1$, and ϵ_{∞} the permittivity at frequencies where $\omega\tau \gg 1$.

The conductivity also follows a first-order law, and a conductivity equivalent of the Debye equation can be easily obtained by beginning with the time-domain expression

$$J(t) = [\sigma_{\infty} + (\sigma_S - \sigma_{\infty})(1 - \exp(-t/\tau))] * E(t) \tag{2.3}$$

where $*$ is the convolution operator. Taking the Laplace transform gives

$$\sigma(\omega) = \sigma_{\infty} + \frac{(\sigma_0 - \sigma_{\infty})}{1 + j\omega\tau}. \tag{2.4}$$

2.4.2 Responses of Real Systems – Conduction & Multiple Relaxations

Only polarization effects were considered in the preceding section. However, conduction mechanisms have to be taken into consideration along with polarization mechanisms to accurately describe the response of real materials. Also, multiple relaxations and distributions of relaxation time have to be taken into consideration.

As can be seen in (2.2), the Debye equation does not include conduction current effects.

Introducing these, the Debye equation can be rewritten as

$$\epsilon = \epsilon_\infty + \frac{(\epsilon_0 - \epsilon_\infty)}{1 + j\omega\tau} - \frac{j\sigma_s}{\omega\epsilon_0}. \tag{2.5}$$

which would imply that the real and imaginary parts of ϵ are

$$\epsilon^{'} = \epsilon_\infty + \frac{(\epsilon_s - \epsilon_\infty)}{1 + (\omega\tau)^2} \tag{2.6}$$

$$\epsilon^{''} = \frac{\sigma_s}{\omega\epsilon_0} + \frac{(\epsilon_s - \epsilon_\infty)}{1 + (\omega\tau)^2}\omega\tau. \tag{2.7}$$

2.4.3 Multiple Relaxation Models – Distribution of Relaxation Times

Due to multiple interaction processes or the presence of more than one type of polar molecule, the dielectric response may be characterized by multiple relaxation time dispersions. A simple instance of this is a dielectric response that may be expressed as multiple Debye terms such that

$$\epsilon = \epsilon_\infty + \frac{(\Delta\epsilon_1)}{1 + j\omega\tau_1} + \frac{(\Delta\epsilon_2)}{1 + j\omega\tau_2} + ... \tag{2.8}$$

where $\Delta\epsilon_n$ corresponds to limits of dispersion characterized by some time constant τ_n. For well separated relaxation times, a plot of the dielectric response will exhibit clearly resolved dispersion regions.

On the other hand, if the relaxation times are not not well separated, the dielectric response will exhibit a broad dispersion. In such a case, the Debye expression becomes

$$\epsilon = \epsilon_\infty + (\epsilon_s - \epsilon_\infty) + \int_0^\infty \frac{\rho(\tau)}{1 + j\omega\tau}\, d\tau. \tag{2.9}$$

where ρ is a distribution function that satisfies the condition

$$\int_0^\infty \rho(\tau)\, d\tau = 1, \tag{2.10}$$

The choice of the distribution function is dependent upon the cause of the multiple dispersions within the material being considered.

In 1941, Cole and Cole [16] proposed what is now widely referred to as the Cole-Cole model:

$$\epsilon = \epsilon_\infty + \frac{\epsilon_s - \epsilon_\infty}{1 + (j\omega\tau)^{1-\alpha}}, \tag{2.11}$$

where α is the distribution parameter within the range $0 \leq \alpha \leq 1$. Note that when $\alpha = 0$ the model simplifies to the Debye Model. The corresponding distribution function is

$$\rho(t/\tau) = \frac{\sin(\alpha\pi)}{2\pi(\cosh[(1-\alpha)\ln(t/\tau)] - \cos(\alpha\pi))}. \tag{2.12}$$

Davidson and Cole proposed a further modification of the Debye equation in 1951 [17] which is as

$$\epsilon = \epsilon_\infty + \frac{\epsilon_s - \epsilon_\infty}{(1 + j\omega\tau)^\beta}. \tag{2.13}$$

In this case, the corresponding distribution is

$$\rho(t/\tau) = \frac{1}{\pi}\left(\frac{t}{\tau - t}\right)^\beta \sin(\pi\beta). \tag{2.14}$$

Substituting a value of $\beta = 1$ would recover the ordinary Debye model.

One more expression used to model dielectric data is the Havriliak-Negami model which

is essentially a combination of the Cole-Cole model and the Cole-Davidson model,

$$\epsilon = \epsilon_\infty + \frac{\epsilon_S - \epsilon_\infty}{(1 + (j\omega\tau)^{1-\alpha})^\beta}. \tag{2.15}$$

The corresponding distribution ρ in this case is given by

$$\rho(t/\tau) = \frac{1}{\pi} \frac{(t/\tau)^{\beta(1-\alpha)} \sin(\beta\theta)}{(t/\tau)^{2(1-\alpha)} + 2(t/\tau)^{1-\alpha} \cos(\pi(1-\alpha)+1)^{(\beta/2)}}, \tag{2.16}$$

where $\theta = \arctan\left(\frac{\sin(1-\alpha))\pi}{((t/\tau)+\cos(1-\alpha)\pi}\right)$.

In principle, the Havriliak-Negami model should be the model employed in the description of dielectric properties. However, it is not used very frequently in practice. As stated earlier, the distributions unfortunately do not reveal very much in the sense of underlying mechanisms. Fortunately, they enable the parametrization of experimental data.

2.5 Free-space Optimization

Simulations run with the head-worn antenna placed in free space are shown in this section. Figure 2.6 shows the resonance of the antenna with all the switches open. Optimization was carried out to find antenna states having a voltage standing wave ratio (VSWR) less than 1.5. The goal of these simulations is to demonstrate the performance of the antenna and illustrate the tunable bandwidth that is achievable with the antenna. As stated earlier, the dimensions of the antenna are an outer radius of 14 cm and a substrate thickness of 1.5 mm. Twenty-two shorting pins are laid out as shown in Figure 2.1. In the simulations the pins are modeled as conducting wire segments that are either included or excluded corresponding to the switches being closed and open respectively.

Genetic Algorithms were briefly touched upon in the previous section. Except stated otherwise, the specifics with regards the genetic algorithm employed in this work are as follows: 1) a population size of 100, 2) a maximum number of generations of 200, 3) a

crossover probability of 70%, 4) a mutation probability of 5%, 5) an elitist selection strategy and 6) a population gap of 95% As is required, all pertinent parameters are made frequency dependent. In particular, the segment length and wire radii are specified such that they vary appropriately with frequency in order the remain within the confines of the thin-wire approximation and segmentation rules. The maximum triangle segment edge-length is set as $\lambda/8$ while the maximum wire segment length is set as $\lambda/10$ (where λ is the wavelength in the appropriate medium).

Optimization frequencies were chosen between 1 GHz and 2 GHz in steps of 100 MHz and simulations were carried with the aim being to obtain VSWR values less than 1.5 for each corresponding frequency. As shown in Figure 2.5, VSWR values less than 1.4 were obtained at all frequencies examined. Thus, acceptable antenna performance was achieved over the frequency range considered.

Considering Figures 2.7 through 2.15, the lowest reflection coefficient value obtained for the free space simulation is -55.89 dB at 1.4 GHz as seen in Figure 2.11.

A rank based comparison is embarked upon at select frequencies. This was done to see if any information could be obtained about a relationship between switch combinations and antenna VSWR performance. Does the presence of certain switch combinations explain the ability of the antenna to function at certain frequencies. Are the switch combinations (or groups thereof) that a crucial to the operation at a particular frequency. Consider Figures 2.18 and 2.20. Both figures exhibit different behaviour as far as the ranking is concerned. In this case of Fig 2.18, there seems to be a consistency in the higher resonances that are maintained. Conversely, Fig 2.20 shows no such trend. The results obtained for similar rankings at 1.3 GHz shown in Figure 2.19 exhibit similar variation as is the case with those at 1.4 GHz. As such, no conclusion can be safely drawn about a correlation between the clusters of switches and operation at one frequency. More work needs to be done to get a conclusive evaluation of this.

Figures 2.21 and 2.22 show pattern plots obtained from the best switch configurations

obtained at 1.1 GHz and 1.3 GHz respectively. The patterns shown are the azimuthal plane patterns, with the azimuthal plane defined in the usual sense as shown in Figure 2.23. In both cases, the patch points in the 0°direction. The results are consistent with expectation based on the fact that the is minimal radiation in the 180°direction which corresponds to back of the ground plane.

2.5.1 Antenna & Head Simulations

After free-space optimizations were carried out, simulations were carried out with the head-worn antenna placed in proximity to the human head model. An initial simulation that is done is with the antenna having all the switches open placed on the head. The result obtained is shown in Fig 2.24. As is expected, the resonance is shifted to a lower frequency due to the loading implications of the presence of the head.

The result obtained from the simulation carried out with the head and the head-worn antenna at 1 GHz is shown in Figure 2.25. Due to computational constraints the simulations could not be carried out at multiple frequency points as is the case with the free-space results that were previously presented.

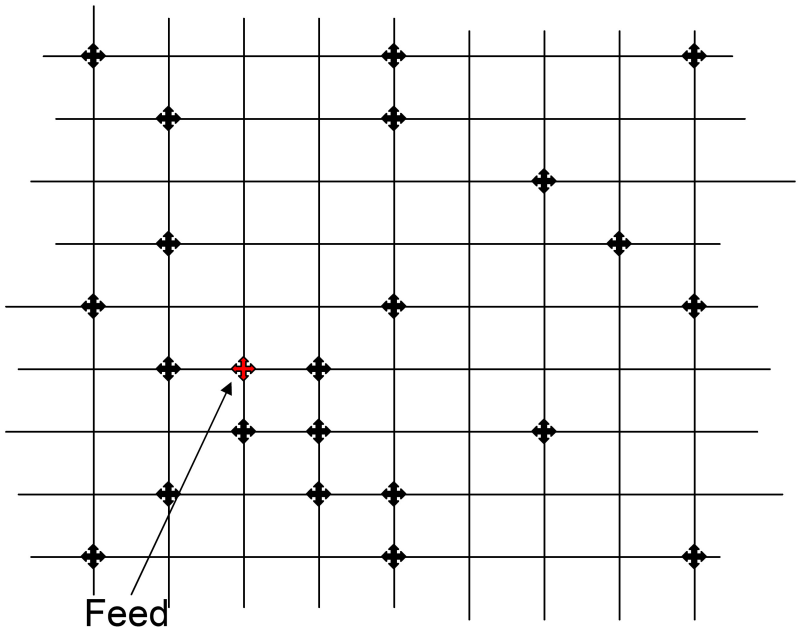

Figure 2.1: The head-worn antenna pin layout. For interpretation of the references to color in this and all other figures the reader is referred to the electronic version of this thesis.

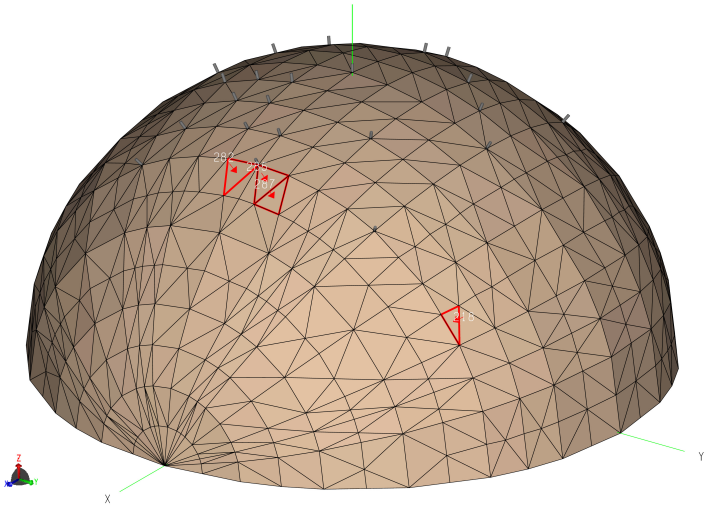

Figure 2.2: Antenna ground plane alone.

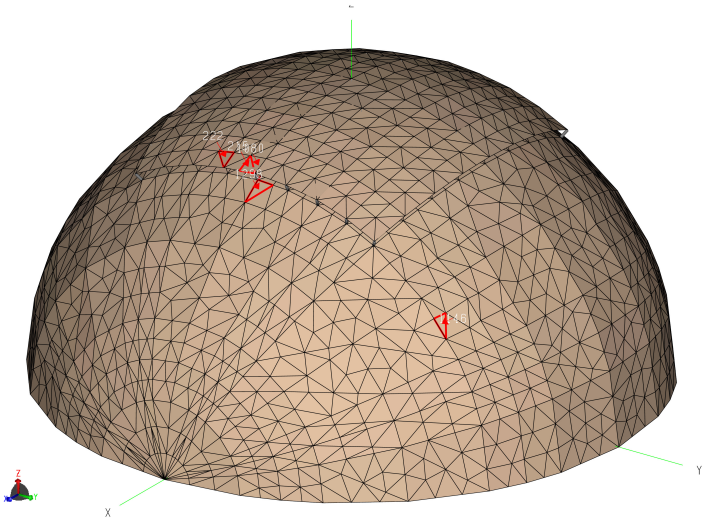

Figure 2.3: Head-worn patch antenna desinged in FEKO

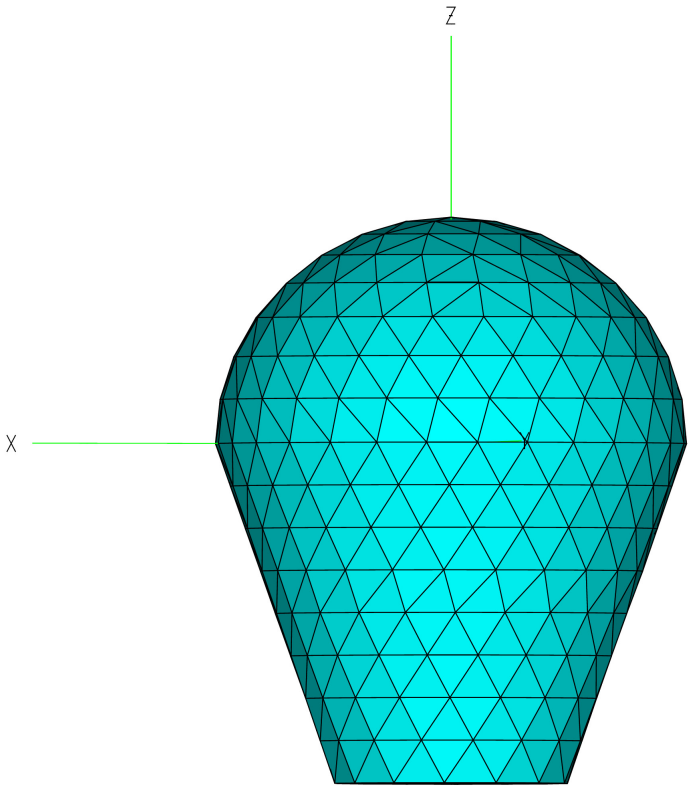

Figure 2.4: Head model in used in FEKO simulations

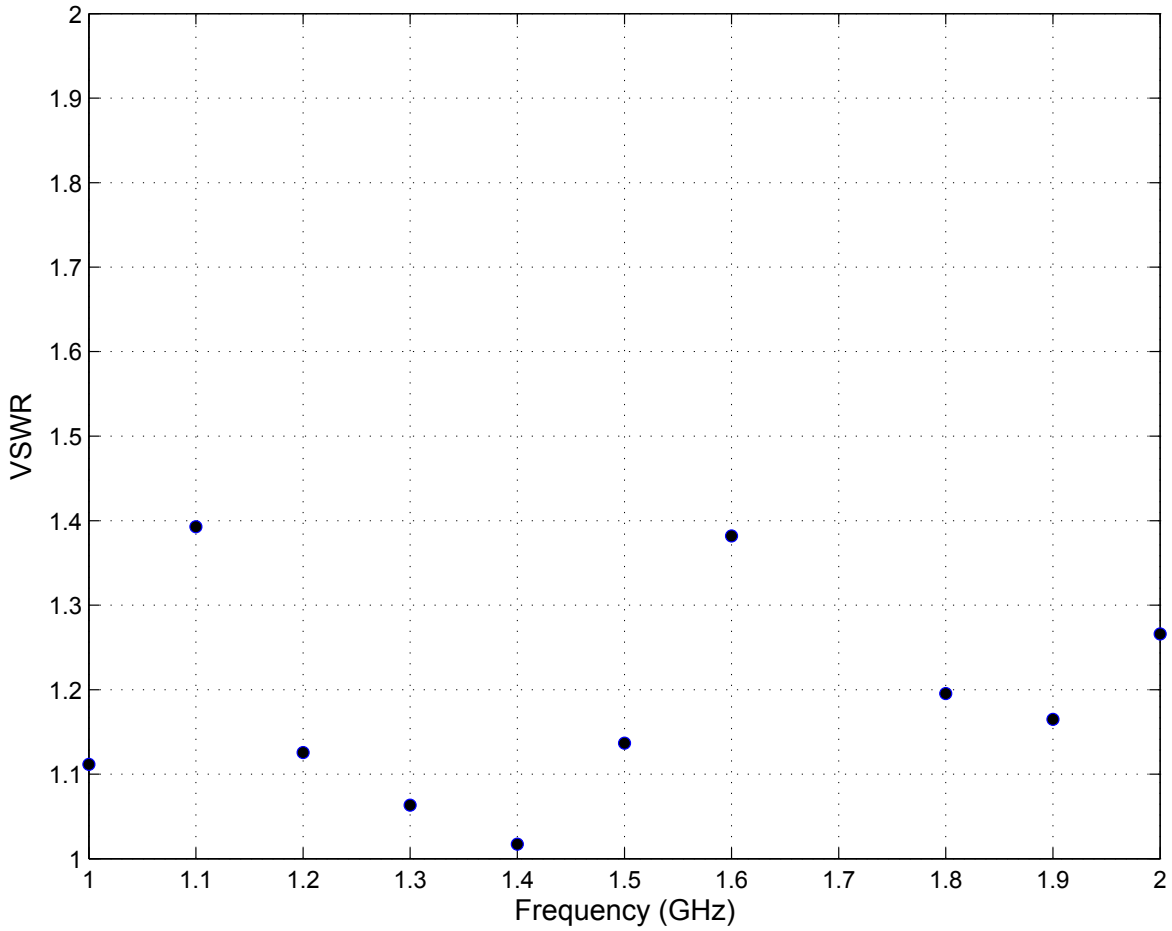

Figure 2.5: Minimum VSWR values obtained for simulated head-worn antenna found using GA search.

Table 2.1: Select permittivity values over the frequency range considered.

Frequency (GHz)	Permittivity	Conductivity
1.0	55.74	1.0062
1.1	55.53	1.0456
1.2	55.35	1.0875
1.3	55.19	1.1318
1.4	55.03	1.1785
1.5	54.87	1.2276
1.6	54.72	1.2792
1.7	54.58	1.3331
1.8	54.44	1.3894
1.9	54.30	1.4480
2.0	54.16	1.5090

Table 2.2: Results from free space simulations of head worn antenna

Frequency (GHz)	VSWR	Resistance (Ω)	Reactance (Ω)	Bandwidth(%)
1.0	1.11152	44.9938	0.3331	2.12
1.1	1.39279	69.6348	-0.4036	2.64
1.2	1.12565	54.1504	-4.5552	3.00
1.3	1.06316	51.3473	2.7960	3.08
1.4	1.01728	50.7645	0.4010	2.57
1.5	1.13664	45.1310	3.6552	4.00
1.6	1.38196	41.8476	12.4272	3.12
1.8	1.19537	51.9860	8.8914	3.5
1.9	1.16478	43.1676	1.9059	3.26
2.0	1.26593	42.6622	-8.0818	2.90

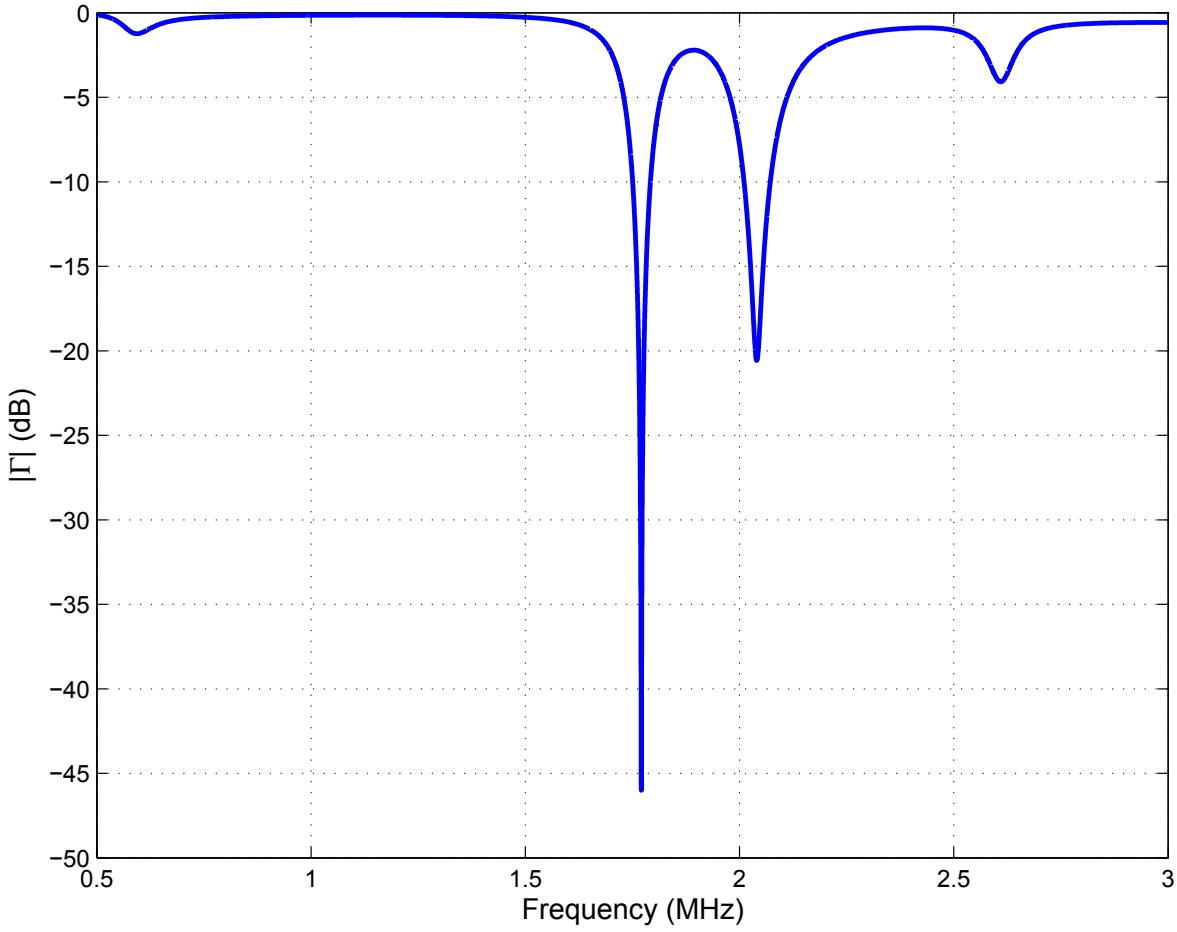

Figure 2.6: Reflection Coefficient of head-worn antenna with all switches open

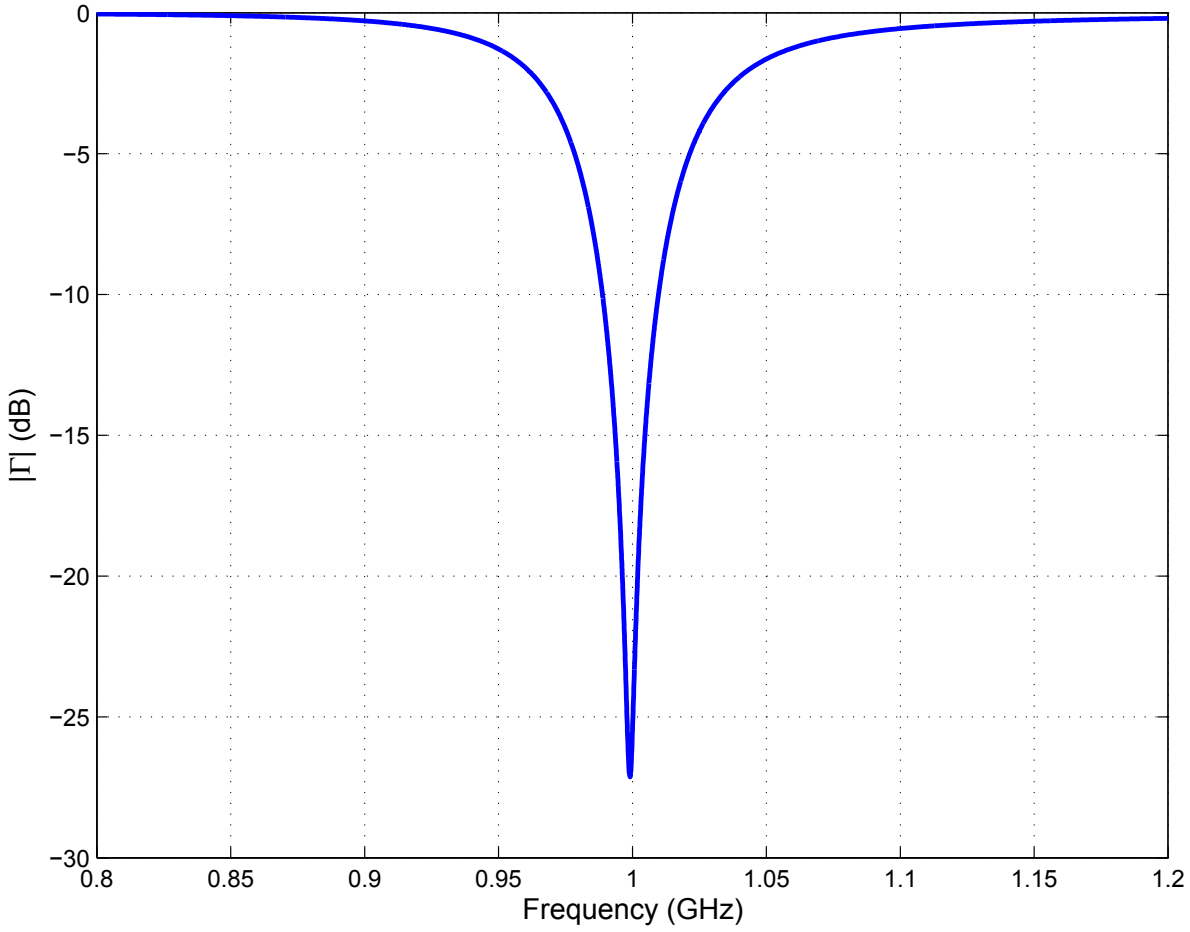

Figure 2.7: Reflection coefficient of head-worn antenna at 1.0 GHz

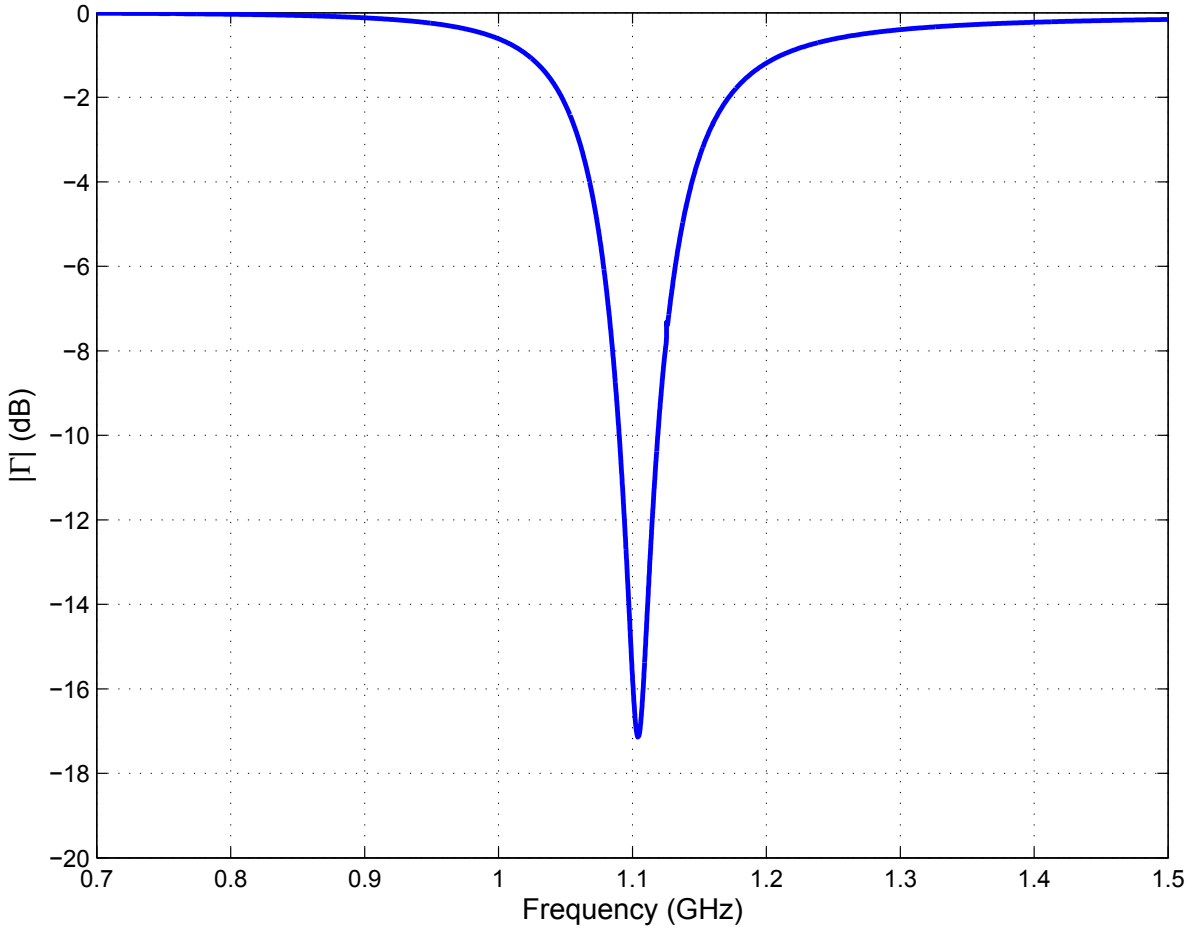

Figure 2.8: Reflection coefficient of head-worn antenna at 1.1 GHz

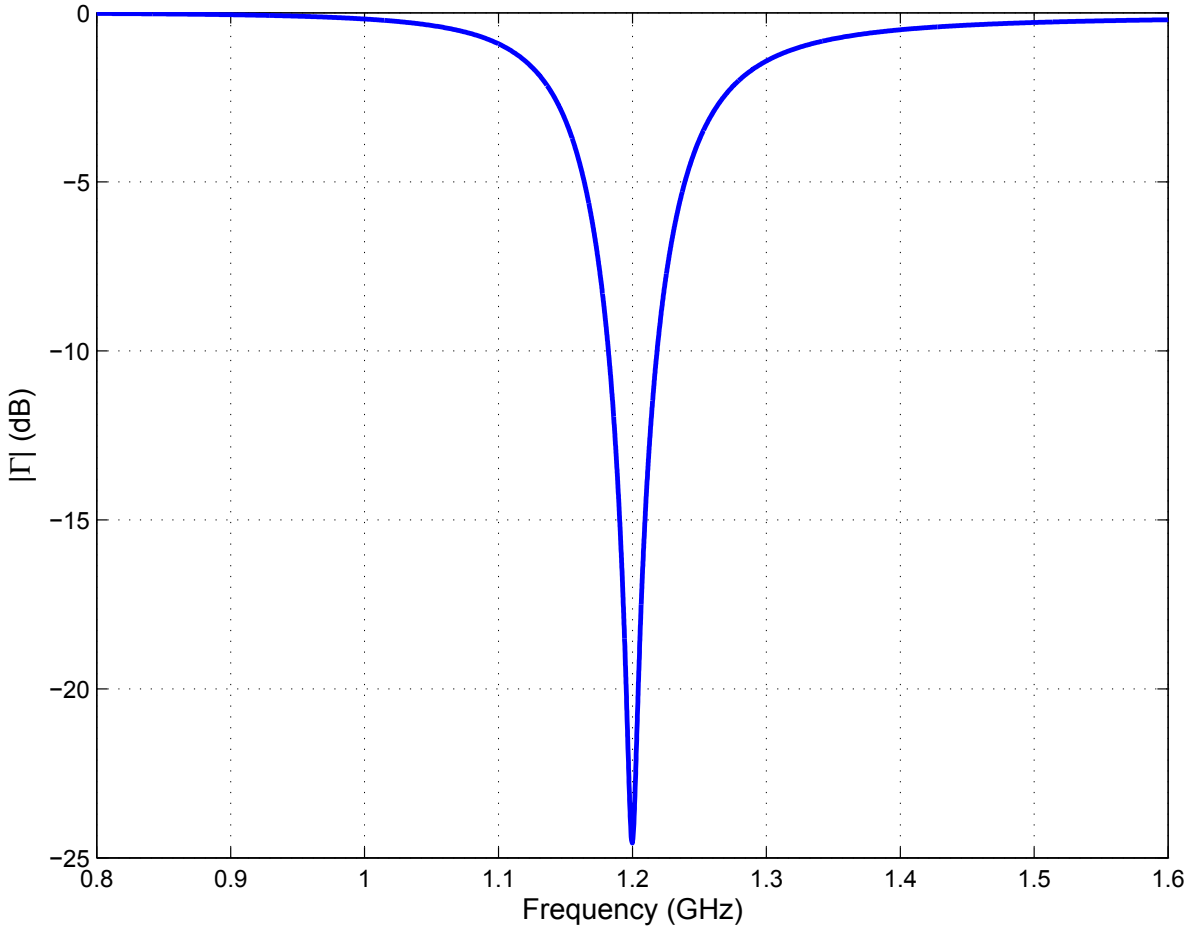

Figure 2.9: Reflection coefficient of head-worn antenna at 1.2 GHz

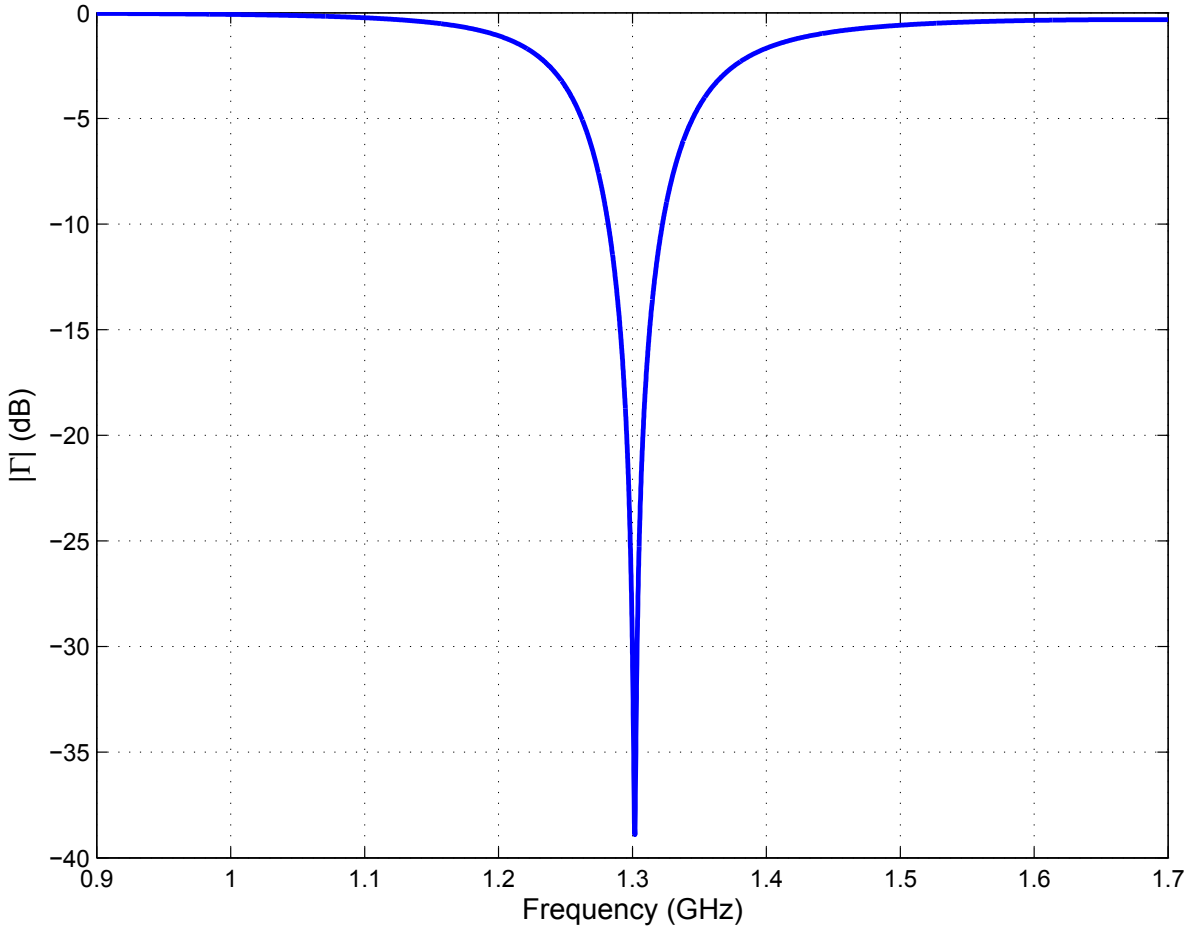

Figure 2.10: Reflection coefficient of head-worn antenna at 1.3 GHz

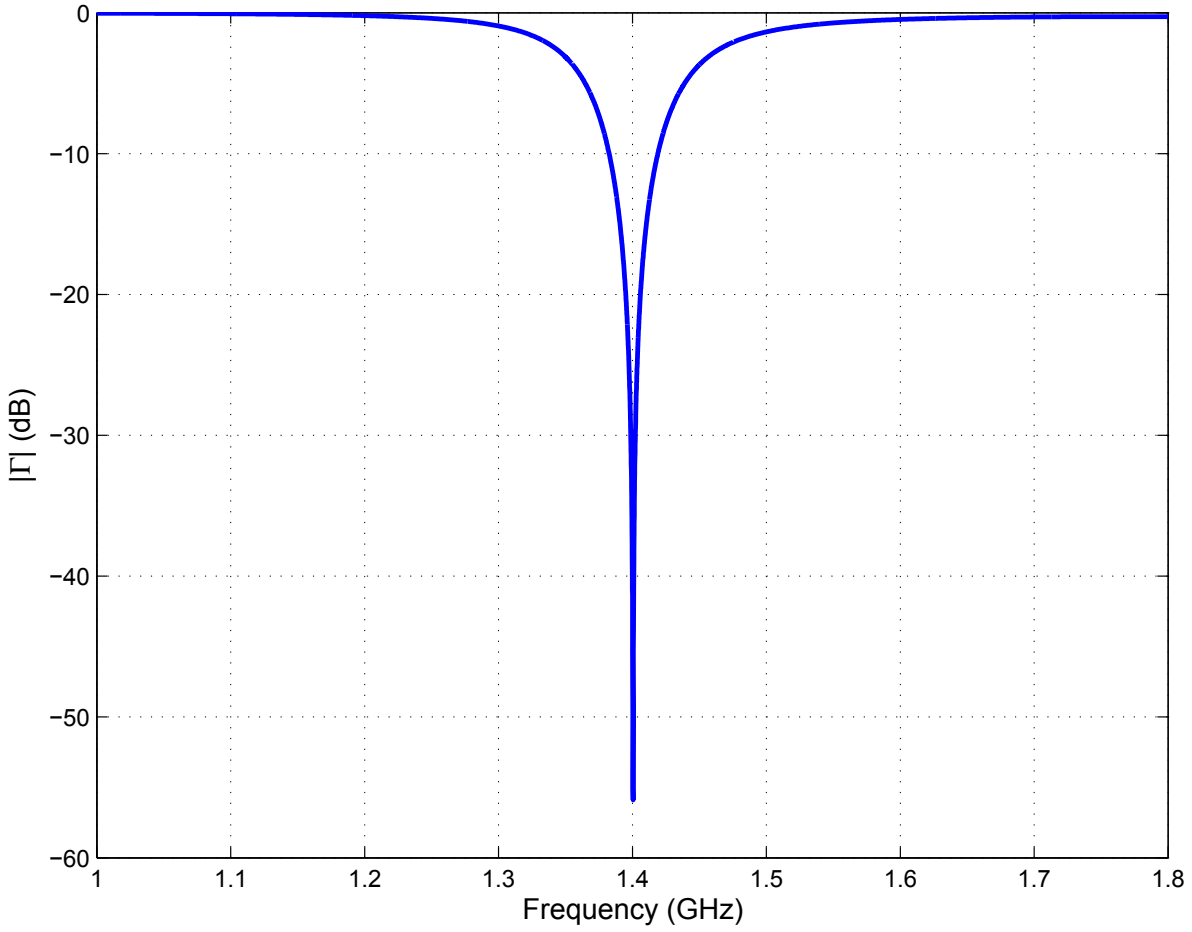

Figure 2.11: Reflection coefficient of head-worn antenna at 1.4 GHz

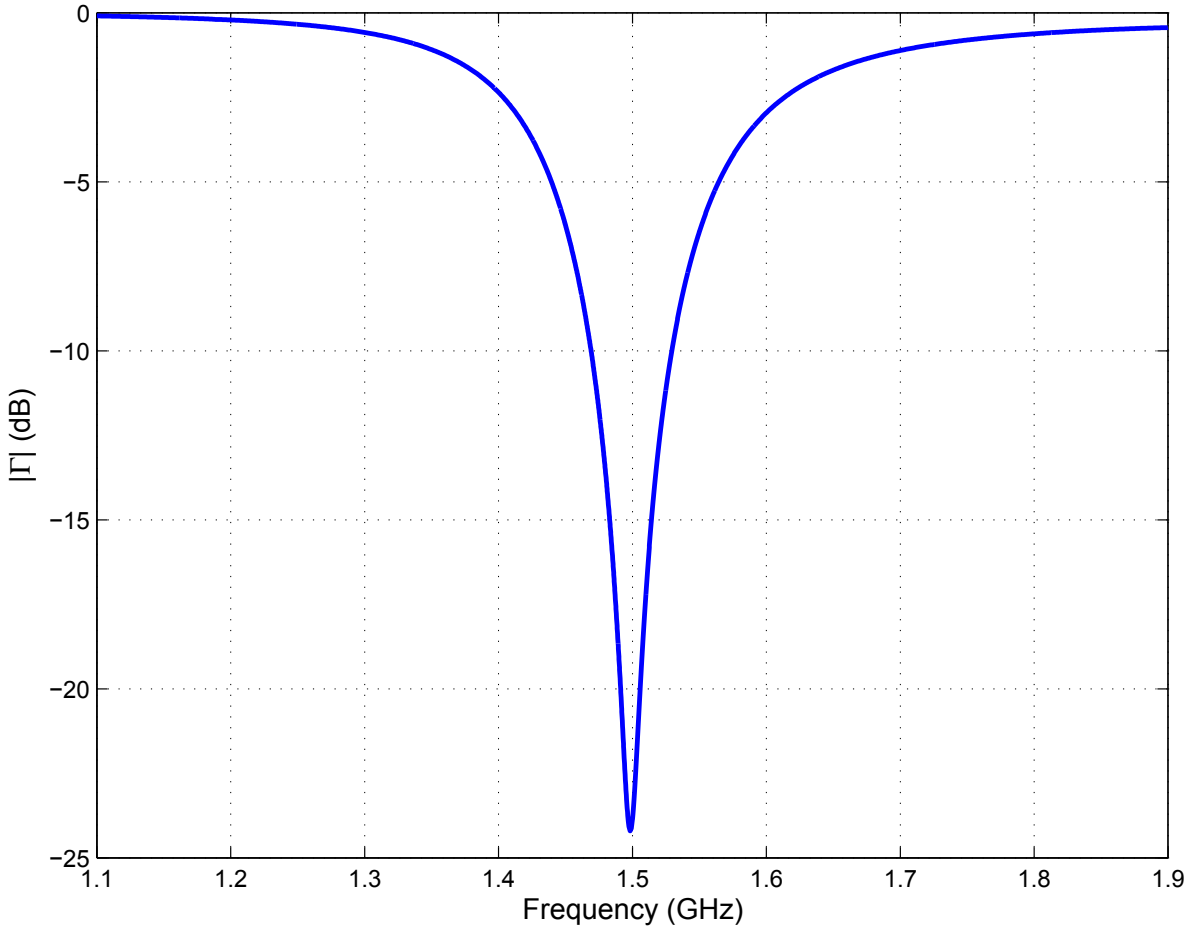

Figure 2.12: Reflection coefficient of head-worn antenna at 1.5 GHz

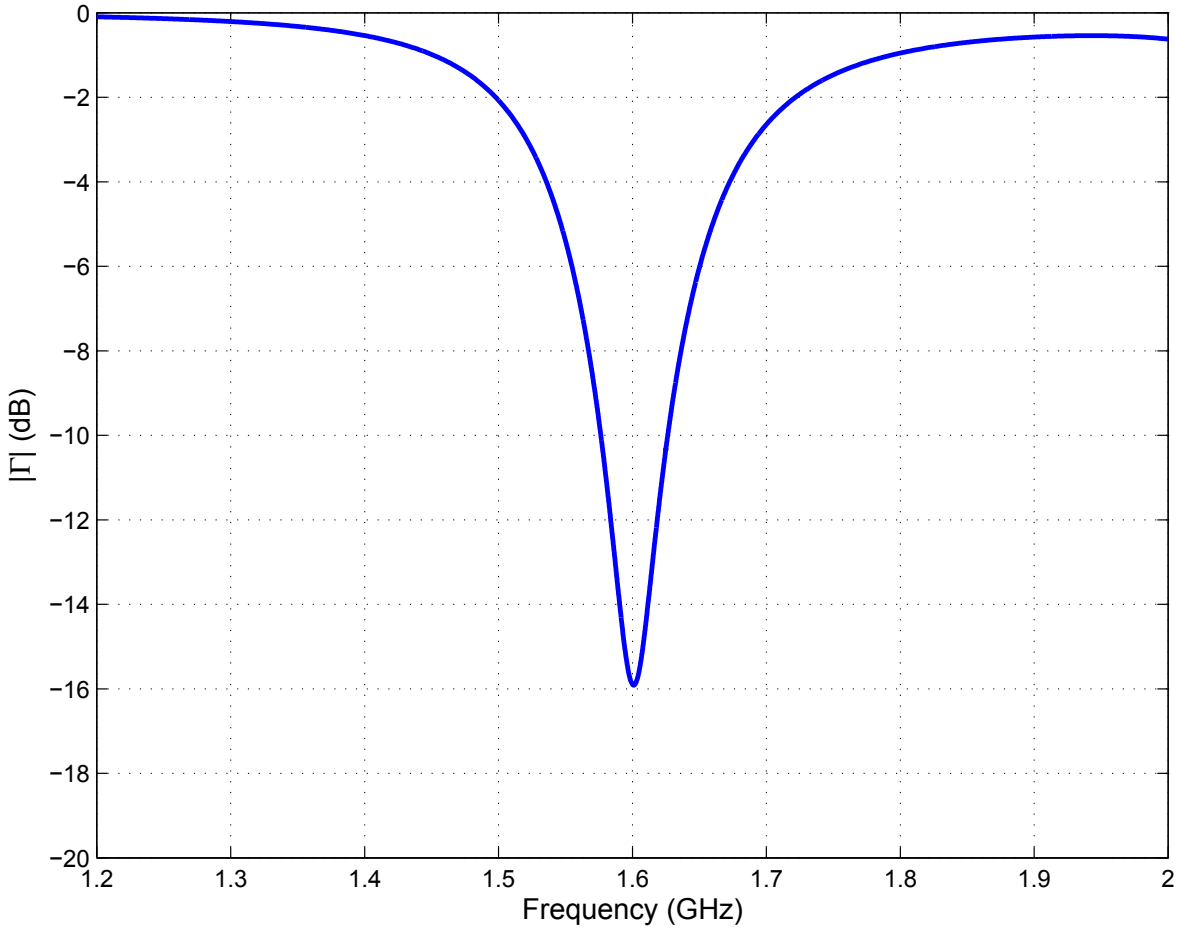

Figure 2.13: Reflection coefficient of head-worn antenna at 1.6 GHz

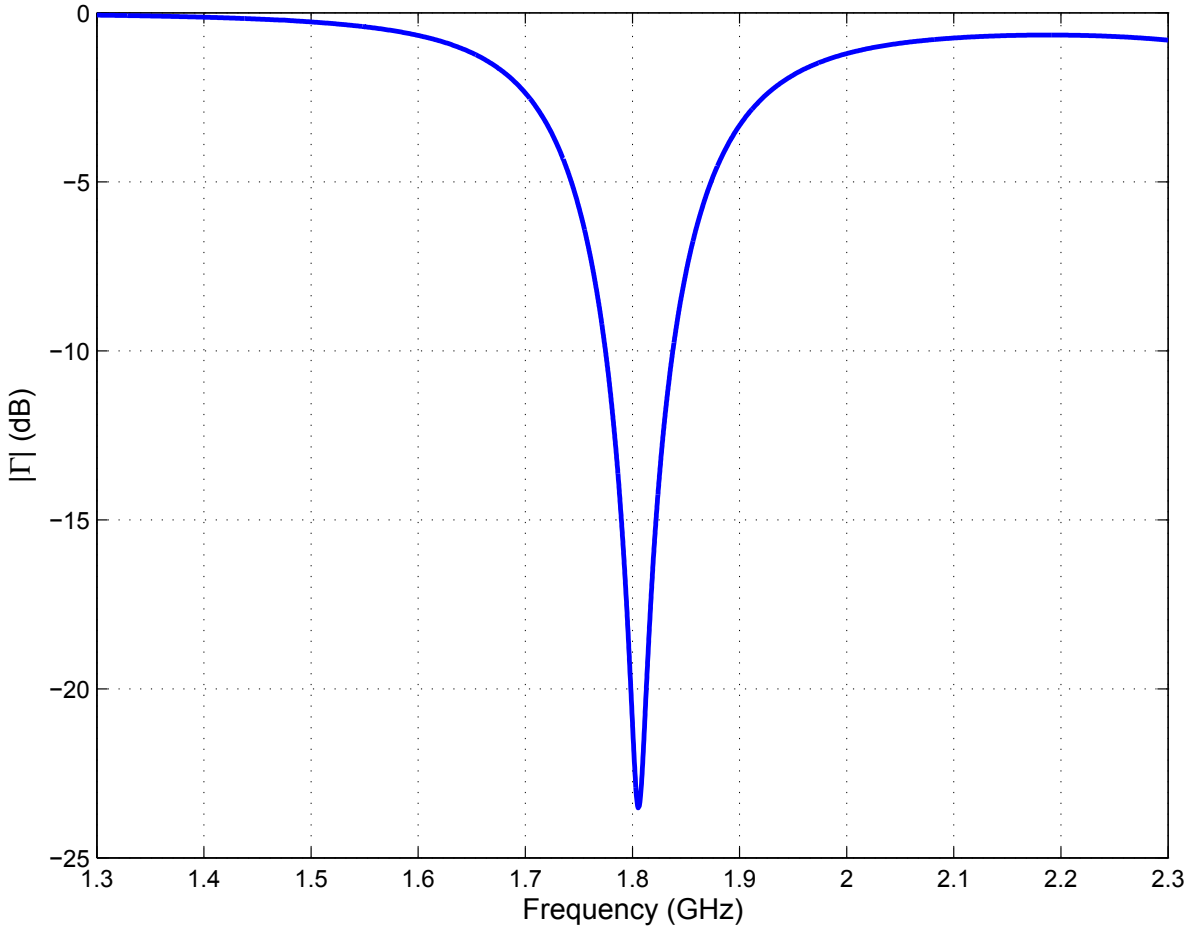

Figure 2.14: Reflection coefficient of head-worn antenna at 1.8 GHz

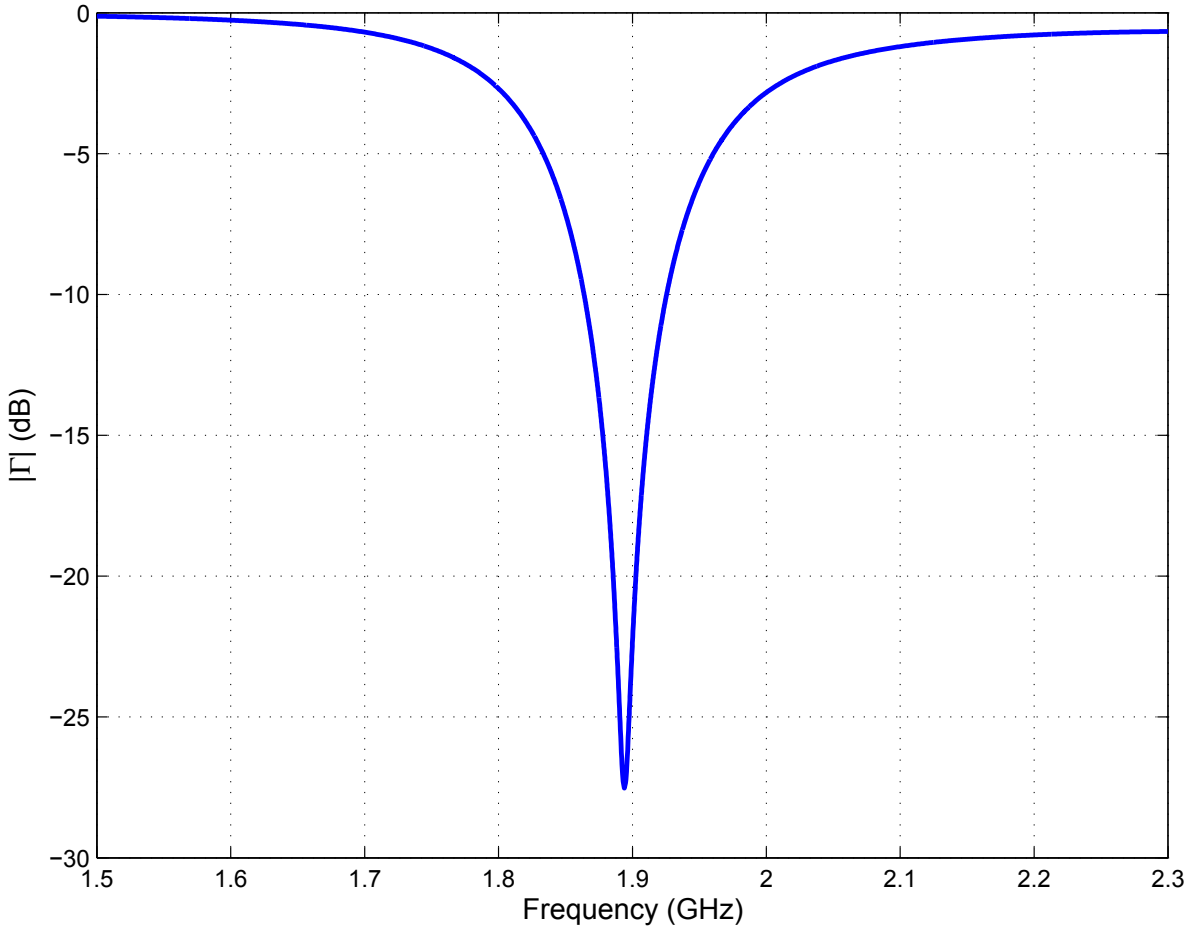

Figure 2.15: Reflection coefficient of head-worn antenna at 1.9 GHz

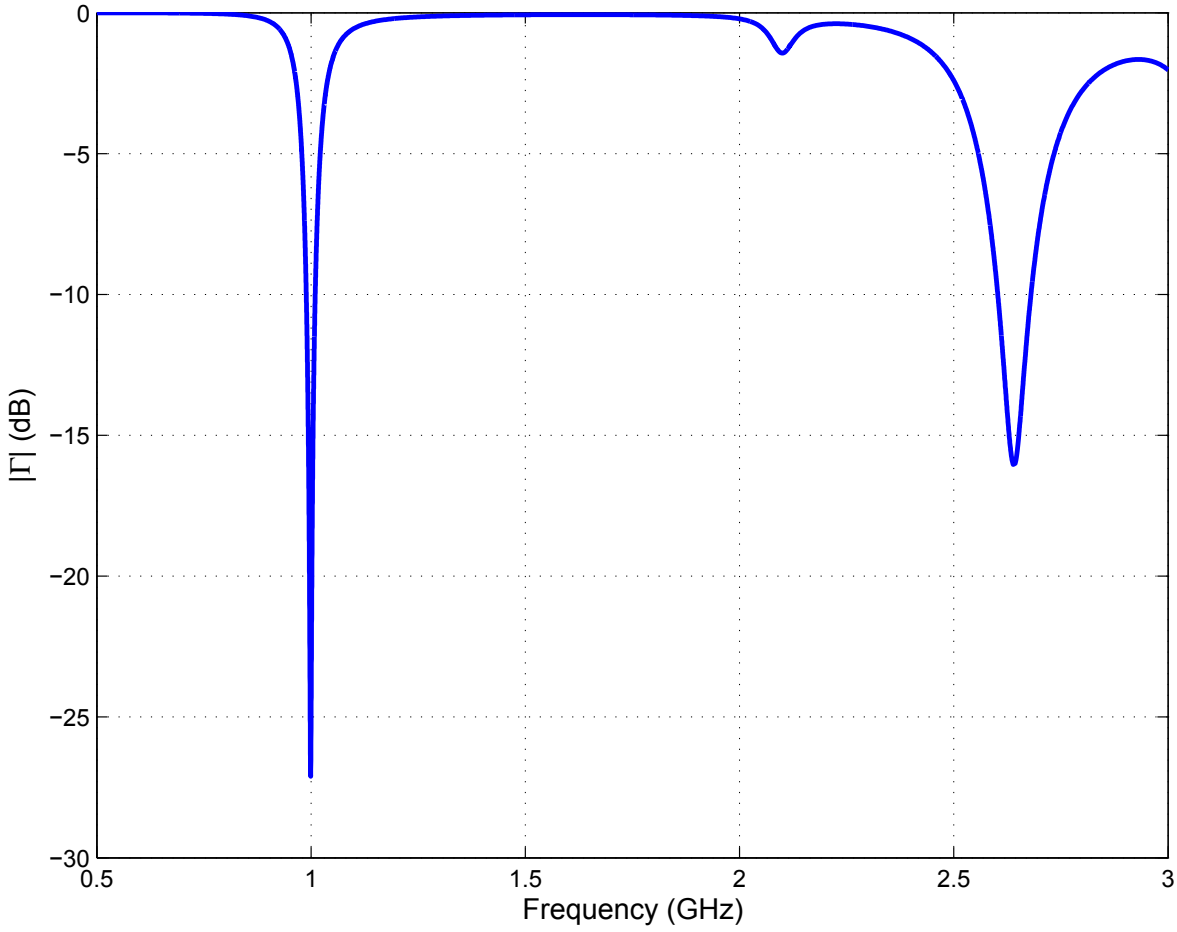

Figure 2.16: Reflection coefficient of head-worn antenna at 1.0 GHz

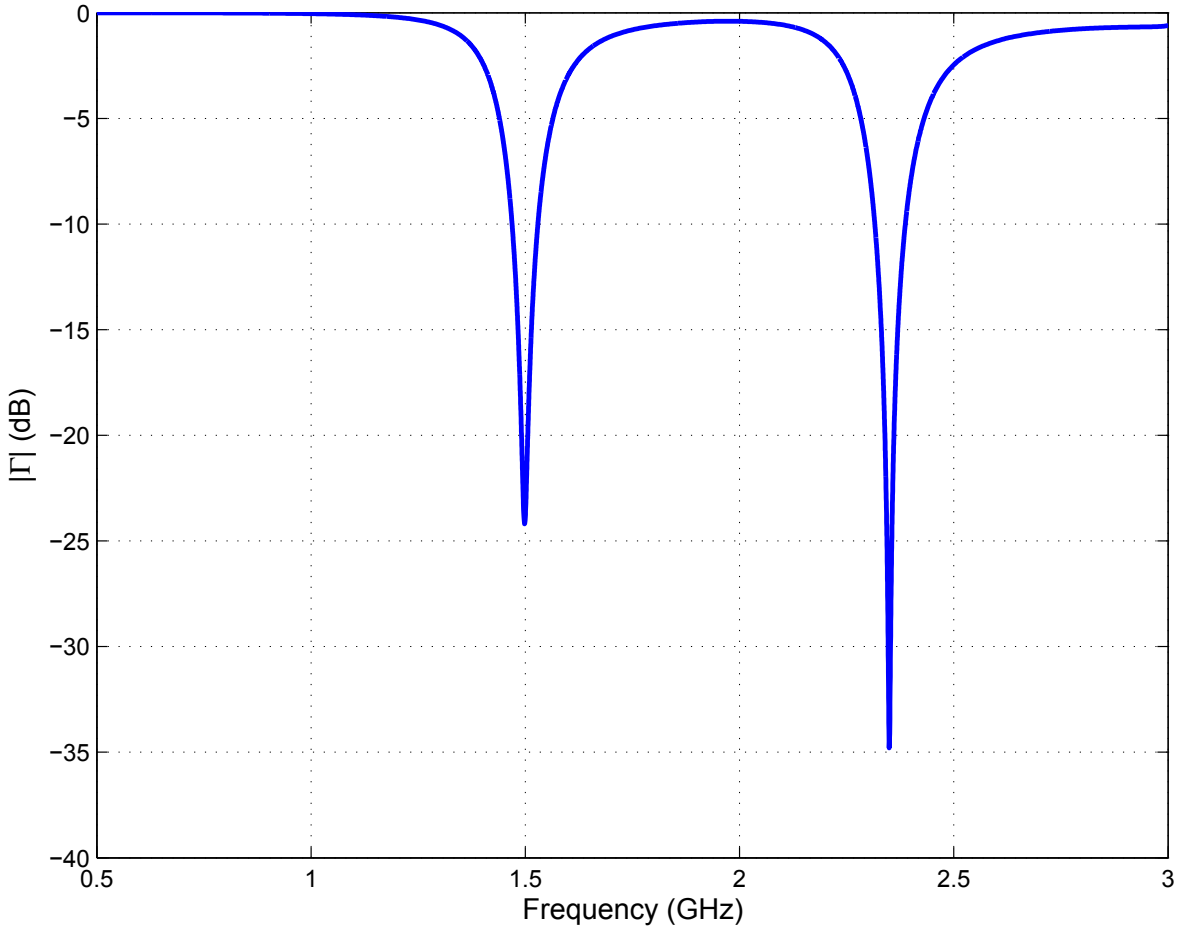

Figure 2.17: Reflection coefficient of head-worn antenna at 1.5 GHz – multiple frequencies

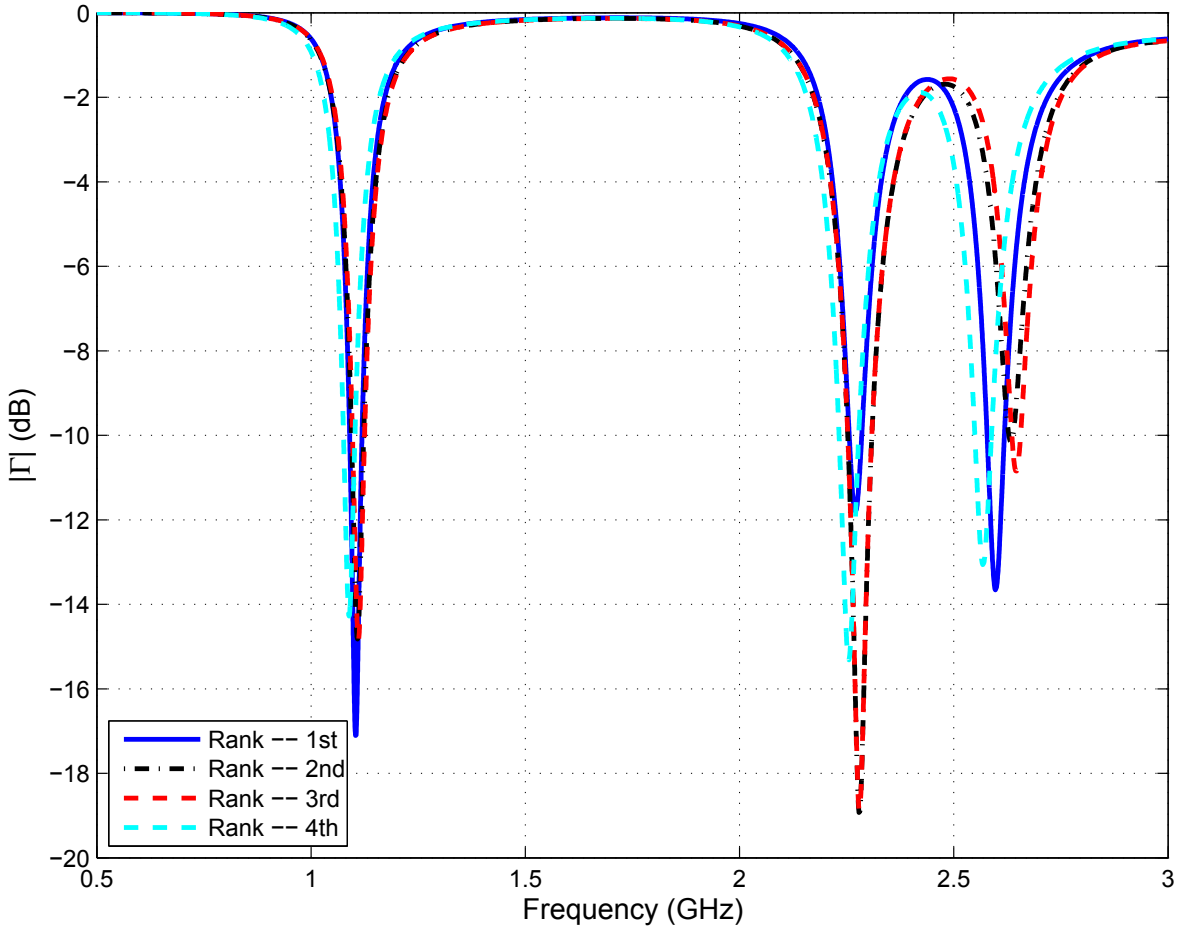

Figure 2.18: Rank comparison at 1.1 GHz

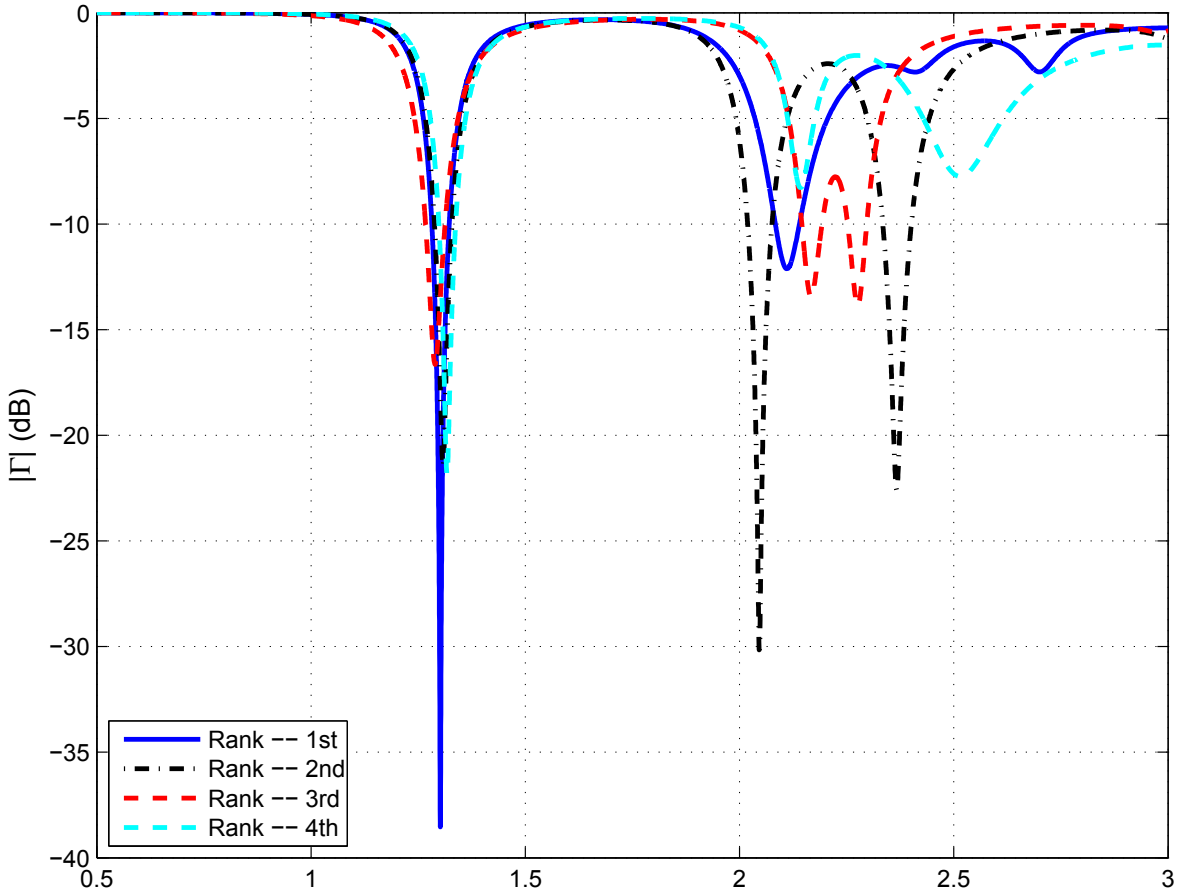

Figure 2.19: Rank comparison at 1.3 GHz

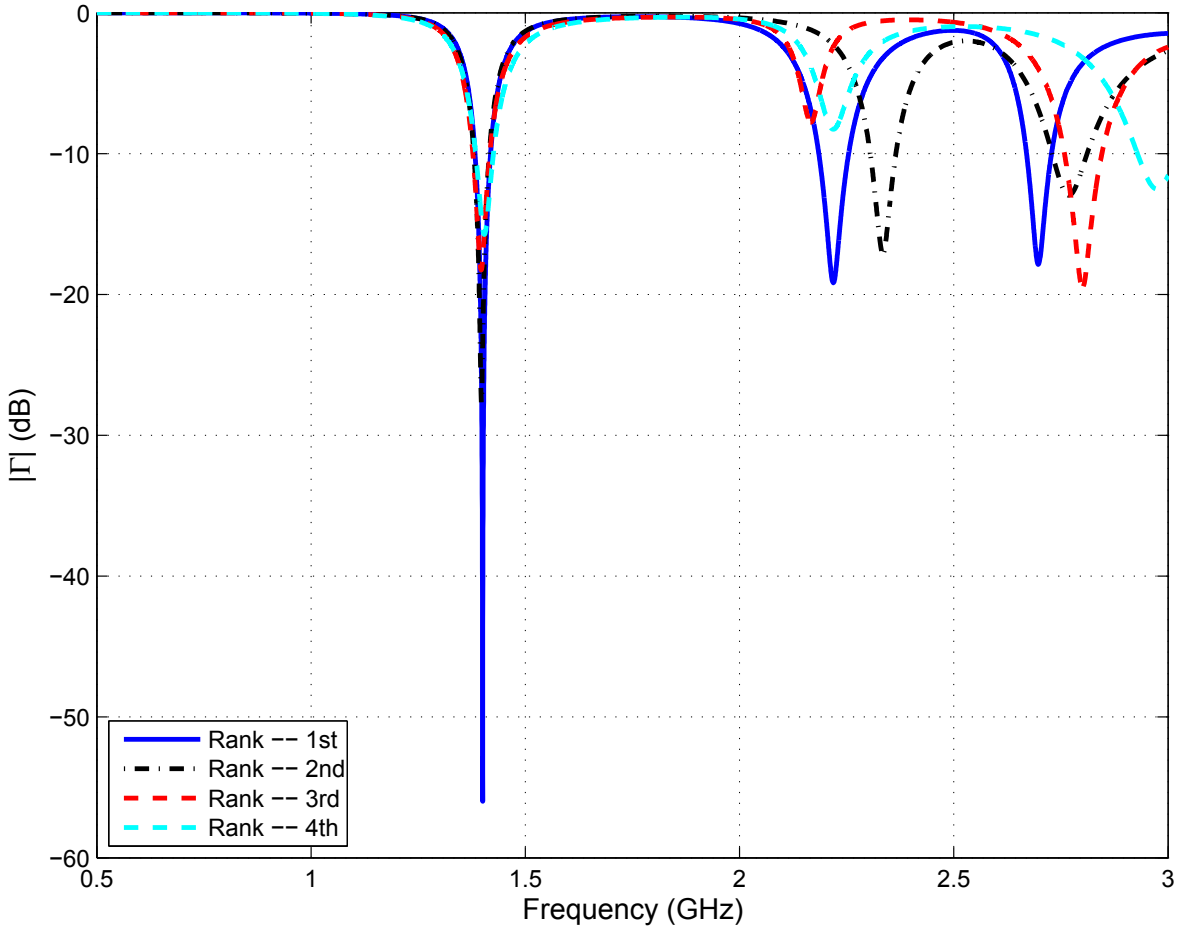

Figure 2.20: Rank comparison at 1.4 GHz

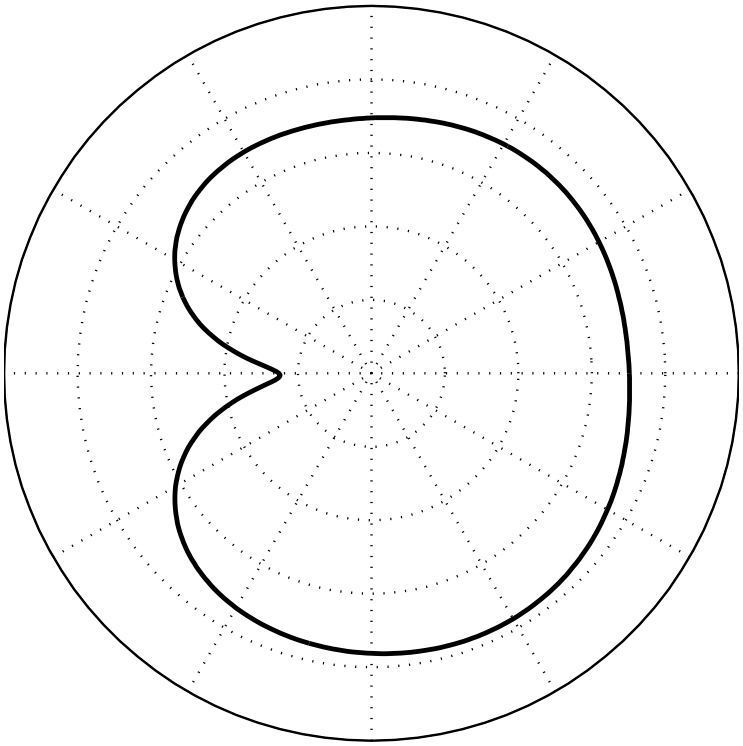

Figure 2.21: Pattern of best state at 1.1 GHz – Azimuthal plane

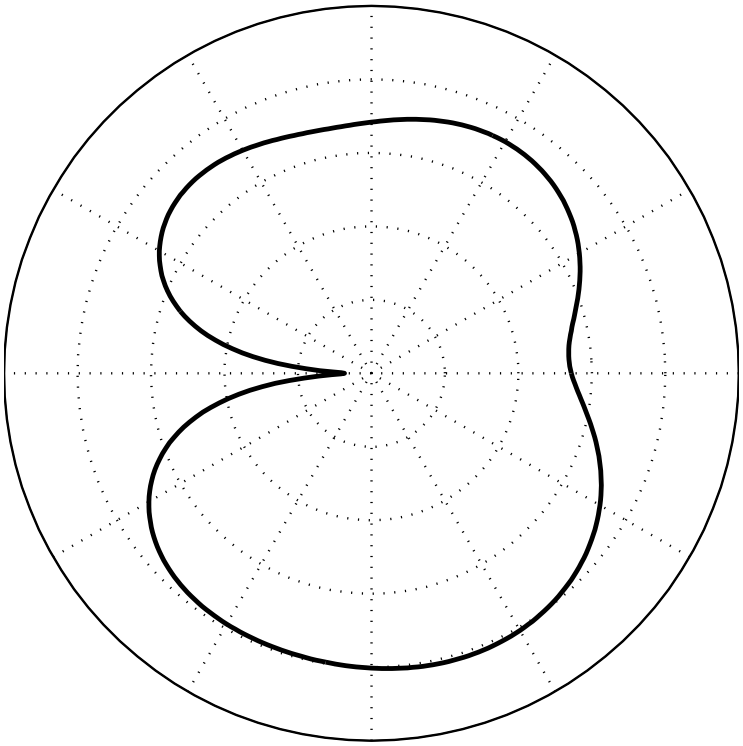

Figure 2.22: Pattern of best state at 1.3 GHz – Azimuthal plane

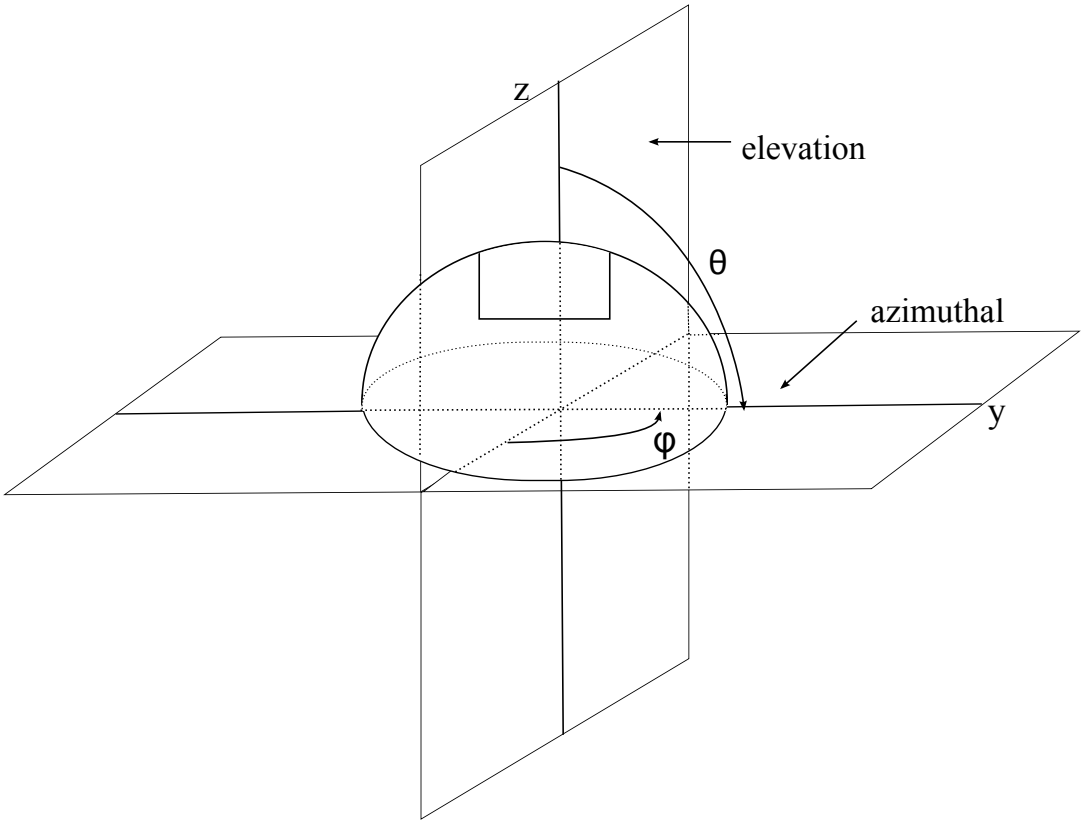

Figure 2.23: Figure illustrating pattern plane measurement designations

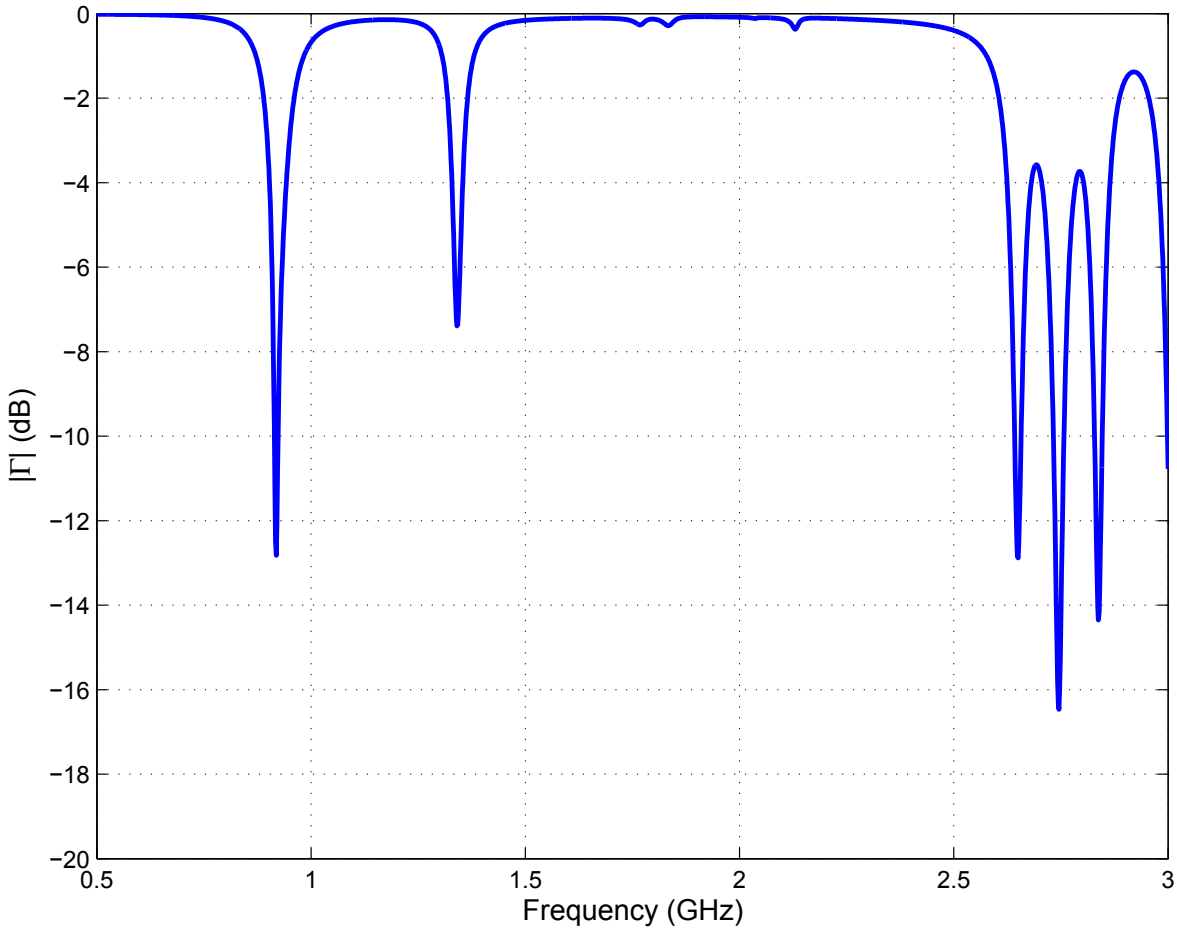

Figure 2.24: Head and antenna with all the switches open

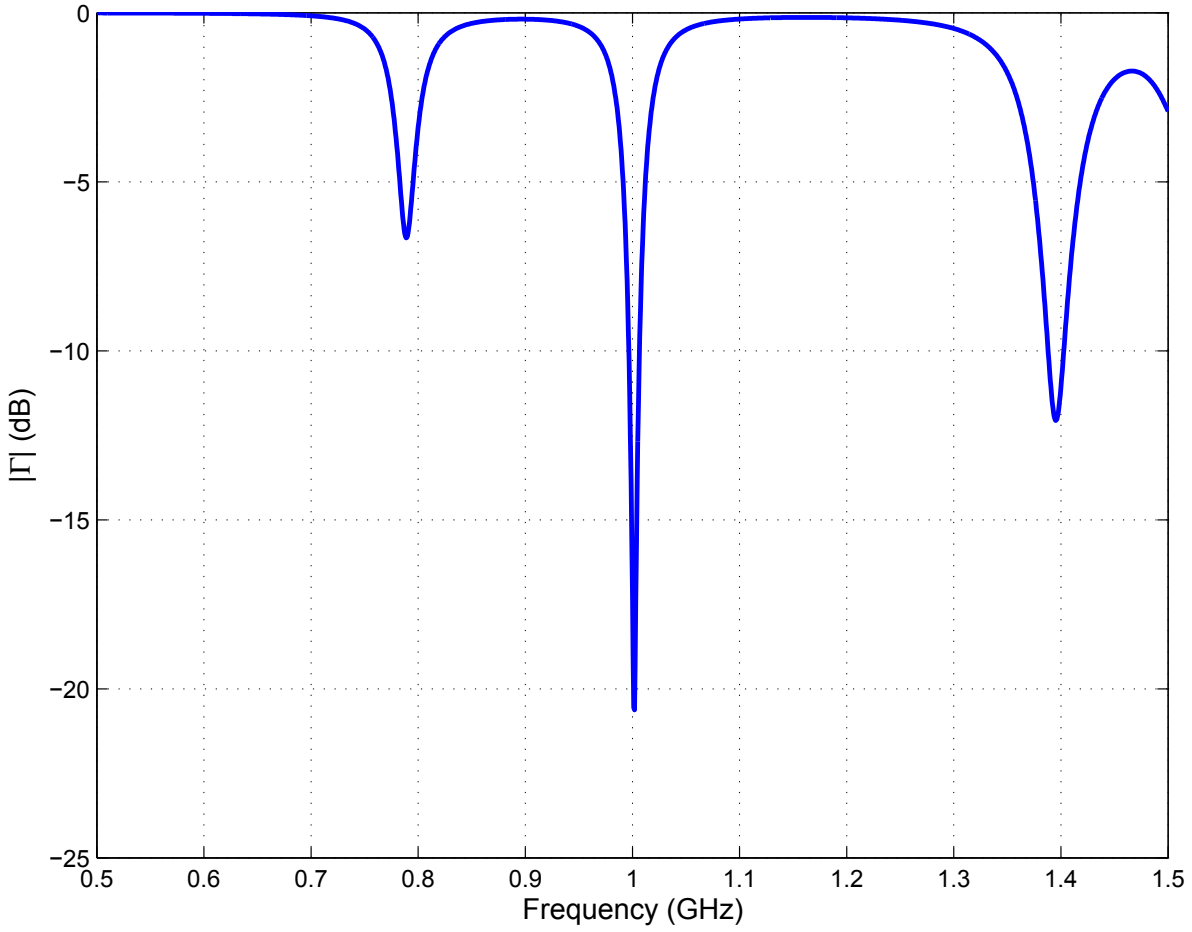

Figure 2.25: Head and antenna at 1.0 GHz

Chapter 3

Measurements

This chapter details experiments that were carried out once the feasibility of the initial proposed antenna concept was established. The general approach taken with the measurements is to start out with an examination of the search space utilizing a random search, before proceeding with optimized measurements at specific frequencies. The point of the random search measurements is to gain a sense of what frequencies would be best for preliminary exploration.

Before going into the details of these experiments, a brief description of the antenna fabrication process is in order.

3.1 Antenna Prototype Fabrication

Two prototypes of the self-structuring head worn antenna were built. In both cases, 22 switches were used just as was done in the simulations. The first prototype of the antenna was built with a substrate region constructed out of layers of papier-maché suspended over a copper ground plane on top of which a copper patch was laid. This was done in order to reproduce closely the air region utilized for the substrate in the simulations. Unfortunately, this iteration of the antenna did not hold up structurally and a need arose for a more rigid substrate region. A picture of this prototype is shown in Figure 3.1.

For the second prototype, a substrate medium made of plastic was decided upon to deal with the structural issues encountered in the prior design. This strayed considerably away from the initial intent to use a substrate medium with a dielectric constant very close to that of free space. However, the desire was to demonstrate a fully functional prototype as a starting point and proceed on to building more sophisticated prototypes. Figure 3.2 shows a picture of the resulting prototype. The switches were laid out in the fashion established for the simulations as shown in Figure 3.3. As shown in Figure 3.4, with all the switches open, the antenna has a principal resonance at 607 MHz. Figure **??** shows an illustration of the antenna and its pertinent dimensions.

Figure 3.5 depicts the experimental setup. A Hewlett-Packard 8753D network analyzer is used for the measurements. A control board powered by a 5 V power supply is used to control the switches. The switches are connected to the computer through a 64 pin ribbon cable having 32 control lines and 32 ground lines. The specification of states is handled by I/O lines from a computer which is connected through the control board. The computer communicates with the network analyzer through a GPIB cable. As can be seen in the figure, the antenna is directly connected to the network analyzer and placed in the anechoic chamber and the required measurements are taken. A standard one-port calibration procedure is carried out before the commencement of each measurement.

Figure 3.6 shows a close-up view of the switch connections. Holes were drilled through the substrate at the positions indicated by the crosses in the figure. A wire was run through each hole with one of the outer leads of the switch soldered to the surface of the patch while the other outer lead was soldered to the ground plane. The inner control leads of the switch were connected to wires that were run to the control board through a ribbon cable. A picture of the control board is shown in Figure **??**.

3.2 Free Space Measurements

3.2.1 Random Search Measurements

Random search measurements were carried out to examine the nature of the resulting search space given the different possible switch combinations for the antenna. The random search measurements were taken from 100 MHz to 1.1 GHz in 100 MHz steps. Figures 3.7 through 3.17 show the measurements taken with 100,000 random states considered at each frequency. These measurements provide insight into the impedance distribution of the available antenna states at the different frequencies considered.

Figure 3.8 is particularly interesting because it suggests a preponderance of states that jointly correspond to constant conductance circles. It is not thought that any significance can be attributed to this since such behavior is not repeated at other frequencies.

The VSWRs for the measured results were combined as shown in Figure 3.18. A close up into the results is shown in Figure 3.19. Based on these results, it can be seen that in the lower frequency range there exists a small frequency span over which it is reasonable to expect a genetic algorithm to easily find good results given a search criterion of a VSWR less than 2. This frequency range is between 100 MHz and 400 MHz. At frequencies above 600 MHz, finding good states with reasonable ease using the genetic algorithm can be similarly expected. In contrast, finding acceptable results using the genetic algorithm would not be as easy between 400 MHz and 600 MHz.

3.2.2 Single frequnecy Optimization

Targeted optimizations were carried out at specific frequencies once the random search measurements were completed. These optimizations were carried out over the same frequency range as the random search measurements. This was done to assess the efficacy of the genetic algorithm relative to the random search. The results obtained are shown in Table 3.1. It is reasonable to expect that in most cases, the genetic algorithm would find a lower VSWR

in fewer looks than the random search. As shown in the table, of the eleven frequencies the random search outperforms the genetic algorithm only at 200 MHz and 600 MHz. For this comparison purpose, the genetic algorithm parameters used were a population size of 50 and a maximum number of generations of 500.

The fact that the genetic algorithm is outperformed at the two aforementioned frequencies does not necessarily preclude its finding desirable states at those frequencies. It is indeed possible that modifying the genetic algorithm parameters could lead to finding more desirable VSWR values at all the frequencies considered. It should also be pointed out that considering the population size and number of generations, a little under 25,000 states are used for the optimizations compared to 100,000 for the random search. It is particularly interesting that one of the "problematic" frequencies is close to the principal resonant frequency of the antenna. Similar behavior is exhibited by the self-structuring patch antenna [23]

Figures 3.20 through 3.22 show reflection coefficient plots for optimizations carried out at arbitrarily chosen frequencies. To begin with, the frequencies chosen are within the lower frequency range for which the random search provided good results. Figure 3.23 suggests the possibility of multiple-frequency optimization with the head-worn antenna.

3.2.3 Pattern Measurements

Pattern measurements were taken to ascertain that the functioning of the head-worn antenna is consistent with expectation for a patch antenna both in the azimuthal plane and the elevation plane. The principal beam of a traditional microstrip patch antenna is in the direction perpendicular to the patch antenna surface. In the direction behind the patch there is typically little radiation but the size of the back lobe is dependent on the extent of the ground plane.

Figures 3.24 through 3.28 show measurements taken at frequencies that were used in the pattern measurements: 200 MHz, 280 MHz & 320 MHz. As can be seen from Figure 3.24, the azimuthal plane pattern obtained at 200 MHz is maximum in the direction perpendicualar

to the center of the patch. On the other hand, the relative field strength is small behind the patch antenna. This is expected given the presence of the ground plane. Similarly, the azimuthal plane pattern at 320 MHz shown in 3.28 shows a similar profile. The azimuthal and elevation planes are designated as shown in Figure 3.29. These patterns are also comparable with those obtained from simulations in Figures 2.21 and 2.22 in the previous chapter.

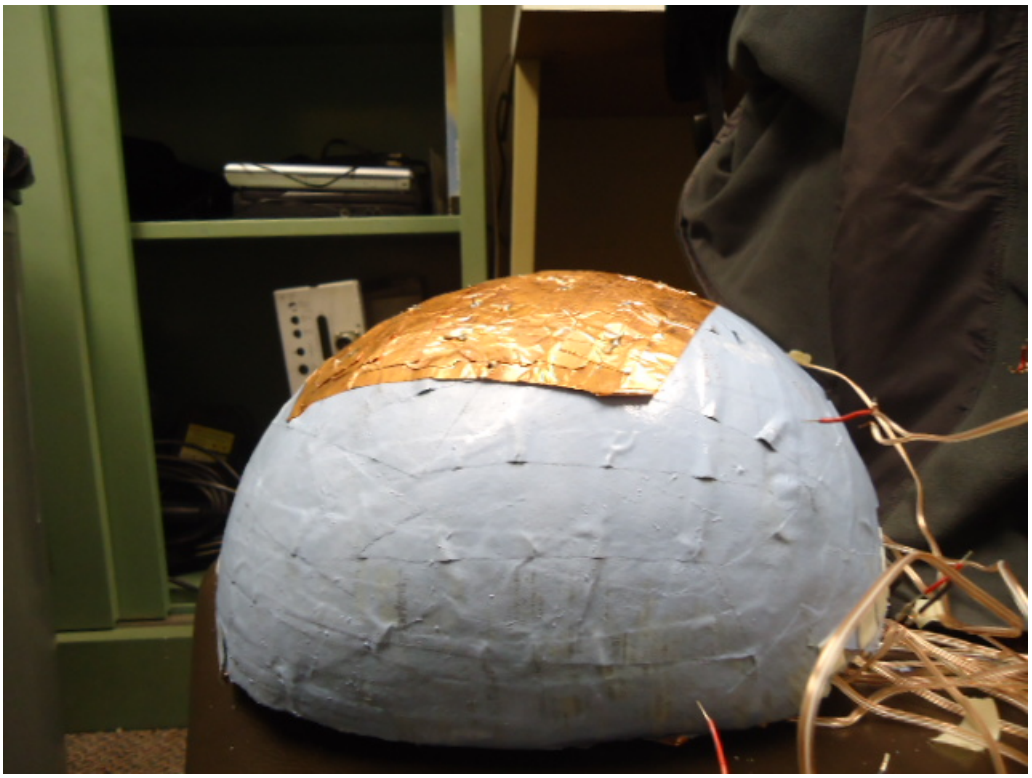

Figure 3.1: Picture of Prototype II

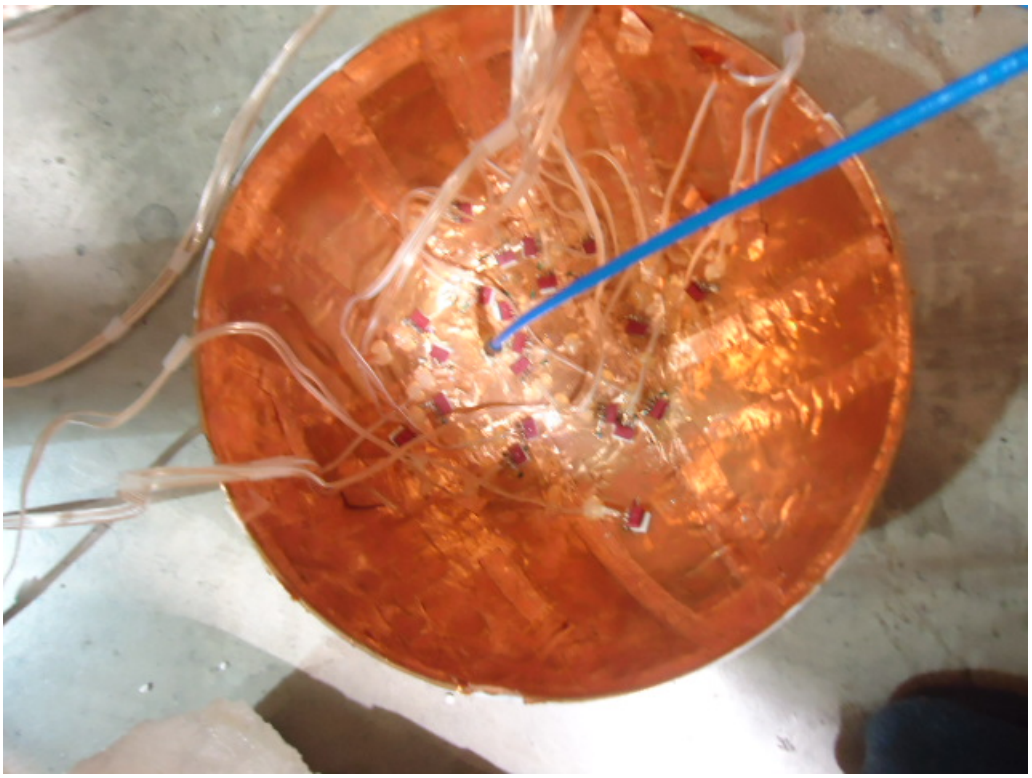

Figure 3.2: Picture of Prototype II

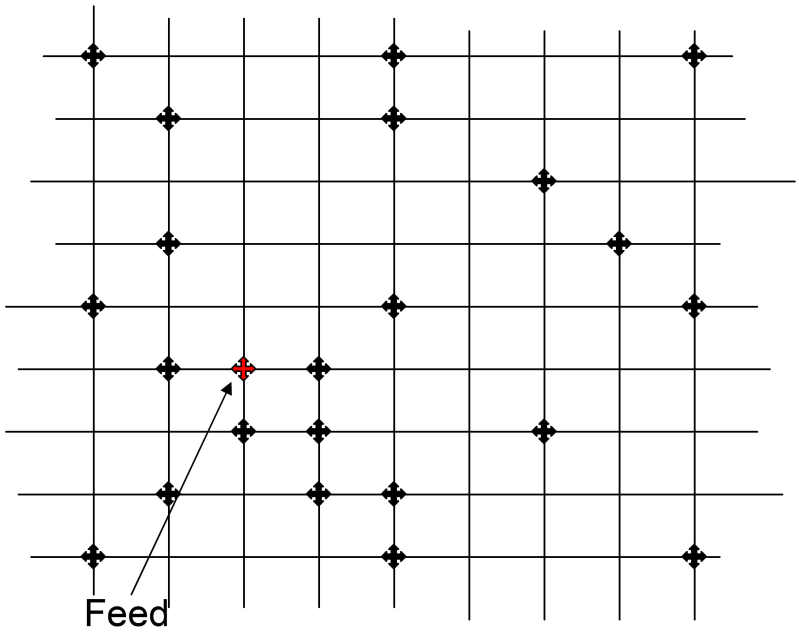

Figure 3.3: Head-worn antenna switch layout

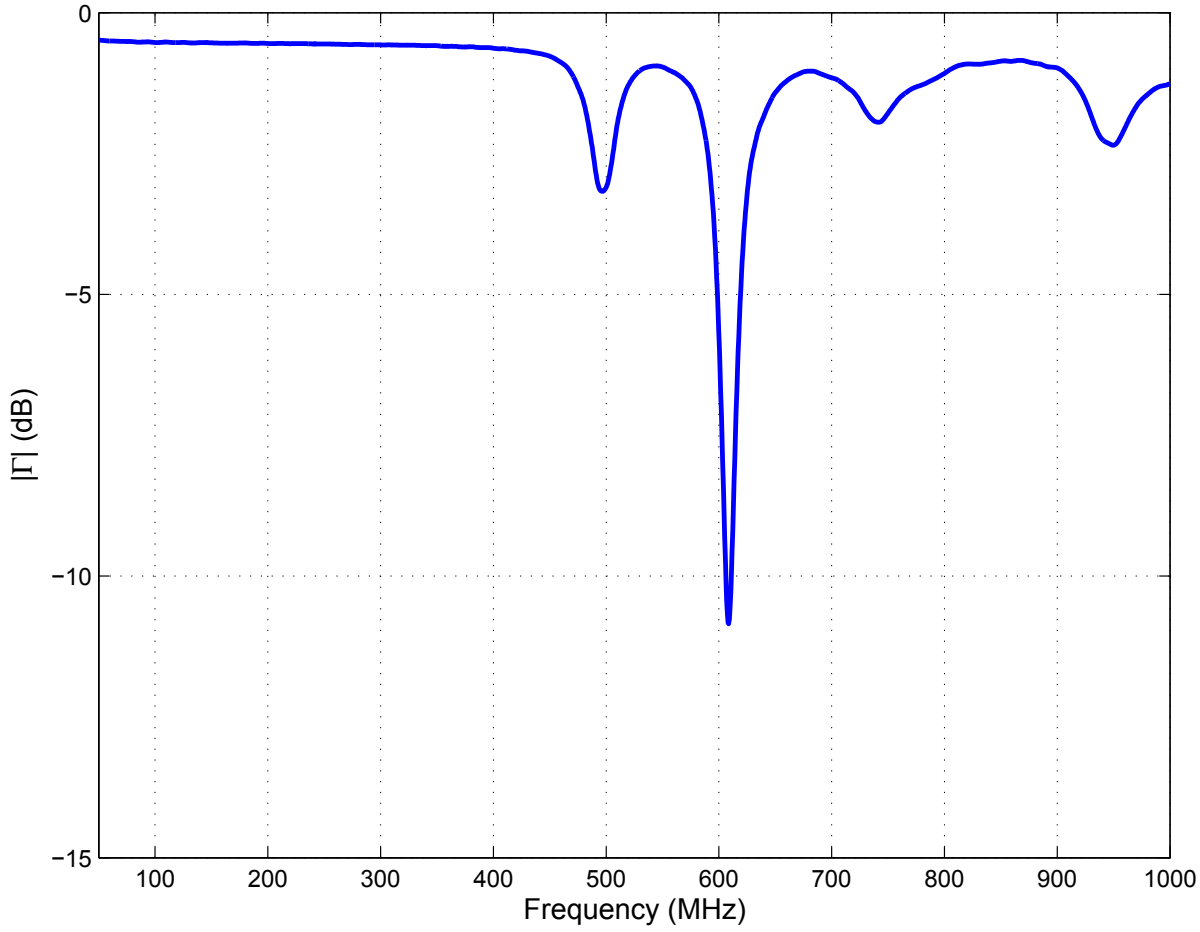

Figure 3.4: Reflection coefficient of antenna with all the switches open

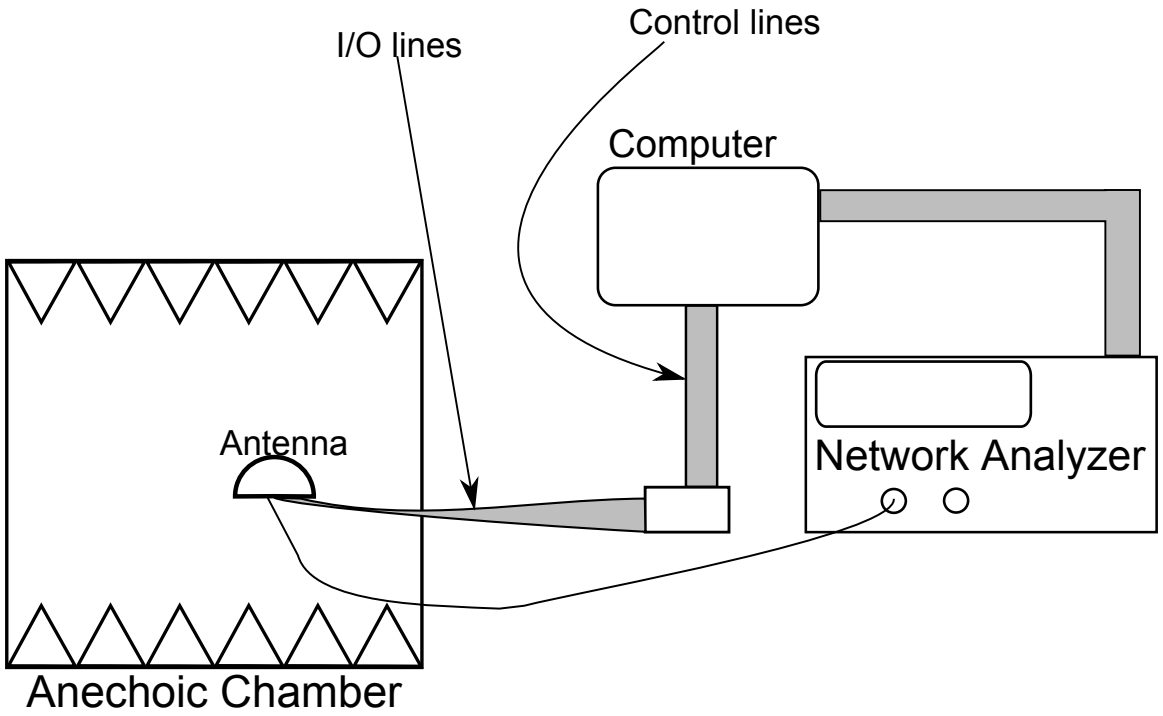

Figure 3.5: Illustration of experimental setup

Figure 3.6: Switch close-up

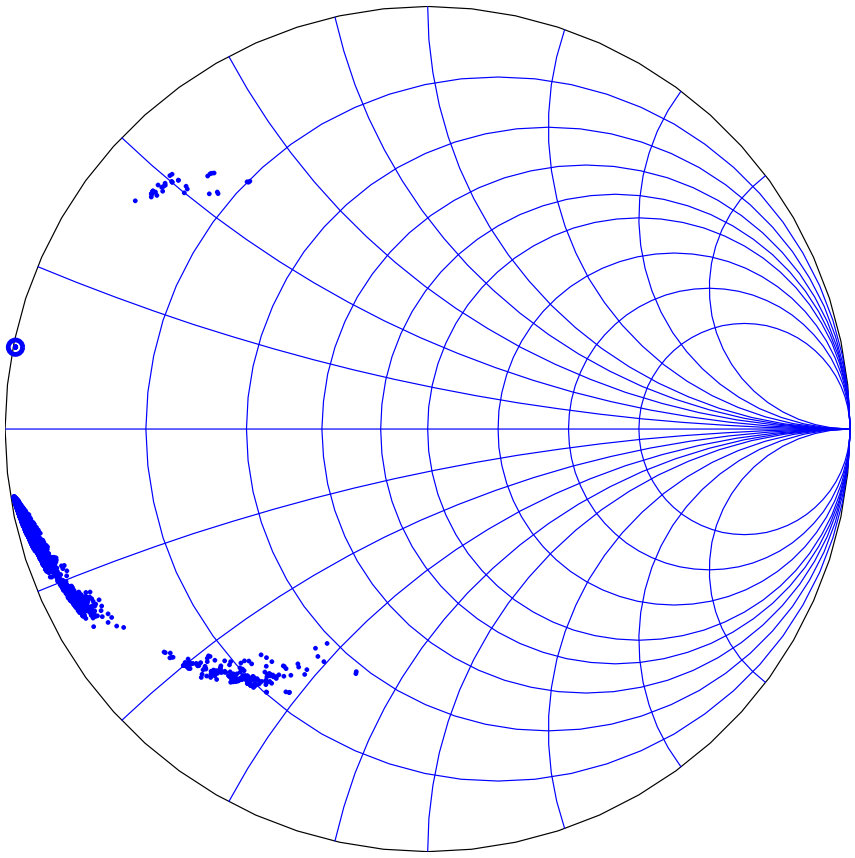

Figure 3.7: Impedances of 100,000 random states at 100 MHz

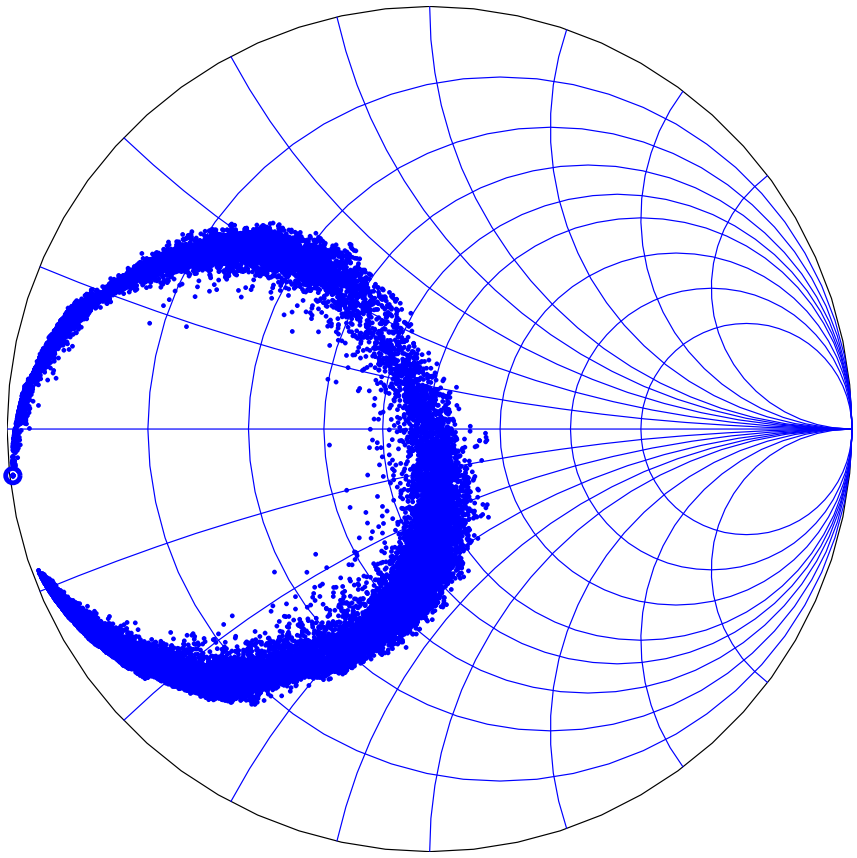

Figure 3.8: Impedances of 100,000 random states at 200 MHz

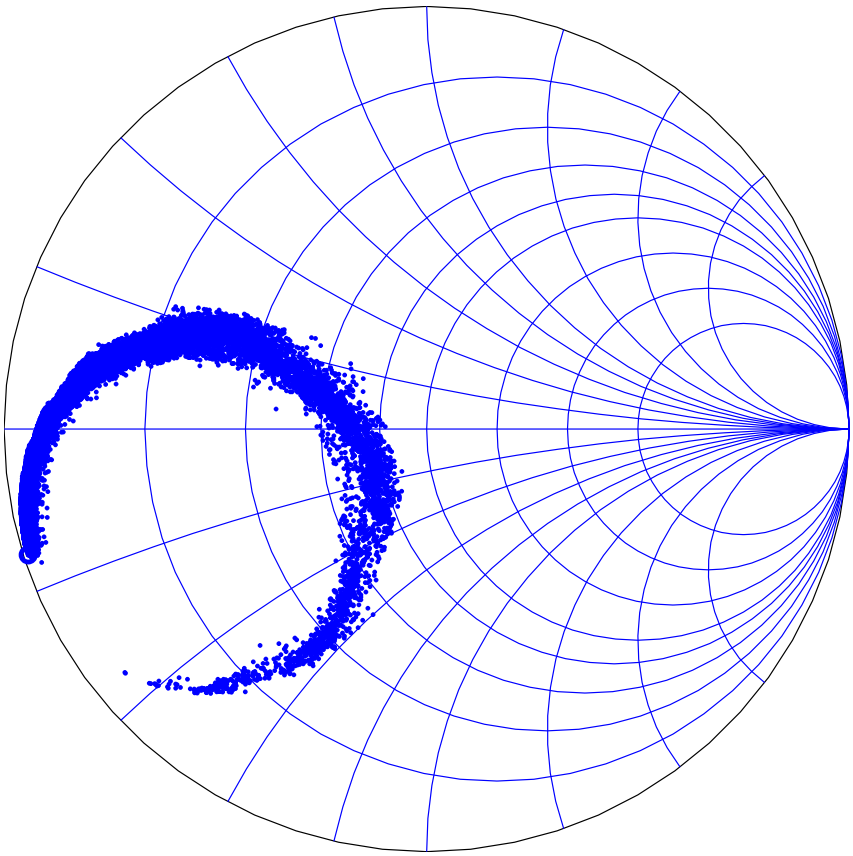

Figure 3.9: Impedances of 100,000 random states at 300 MHz

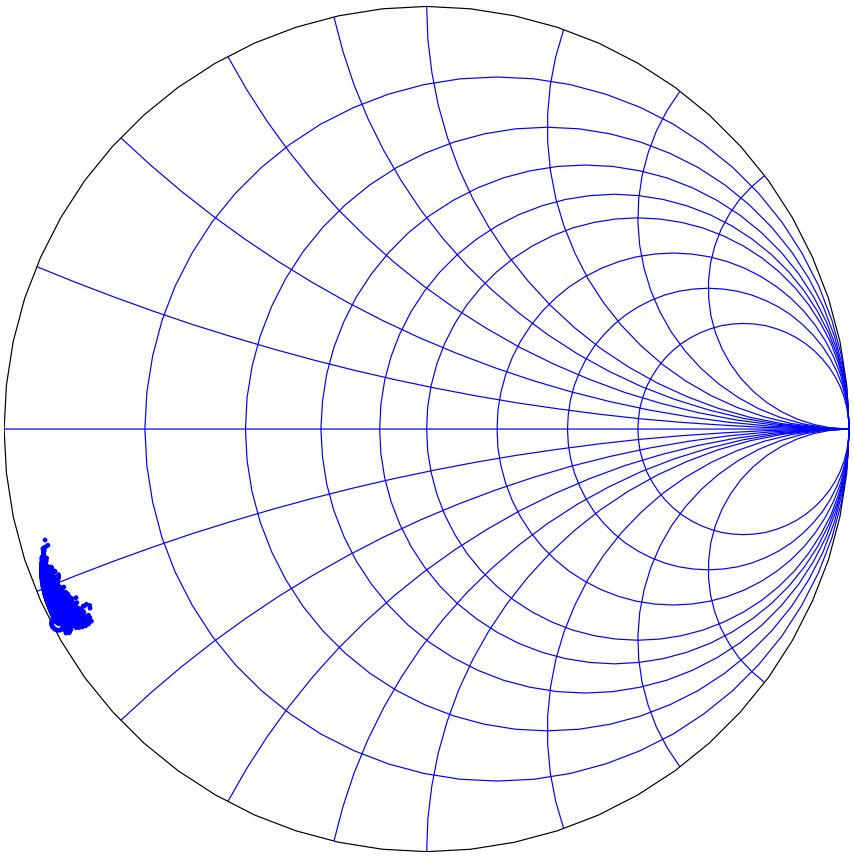

Figure 3.10: Impedances of 100,000 random states at 400 MHz

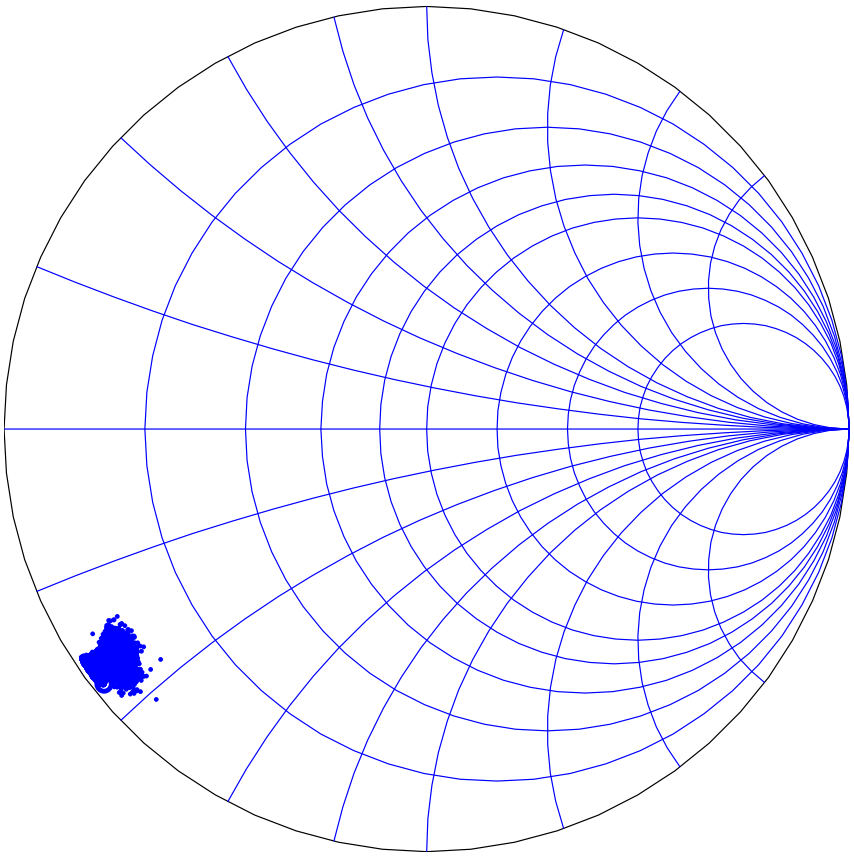

Figure 3.11: Impedances of 100,000 random states at 500 MHz

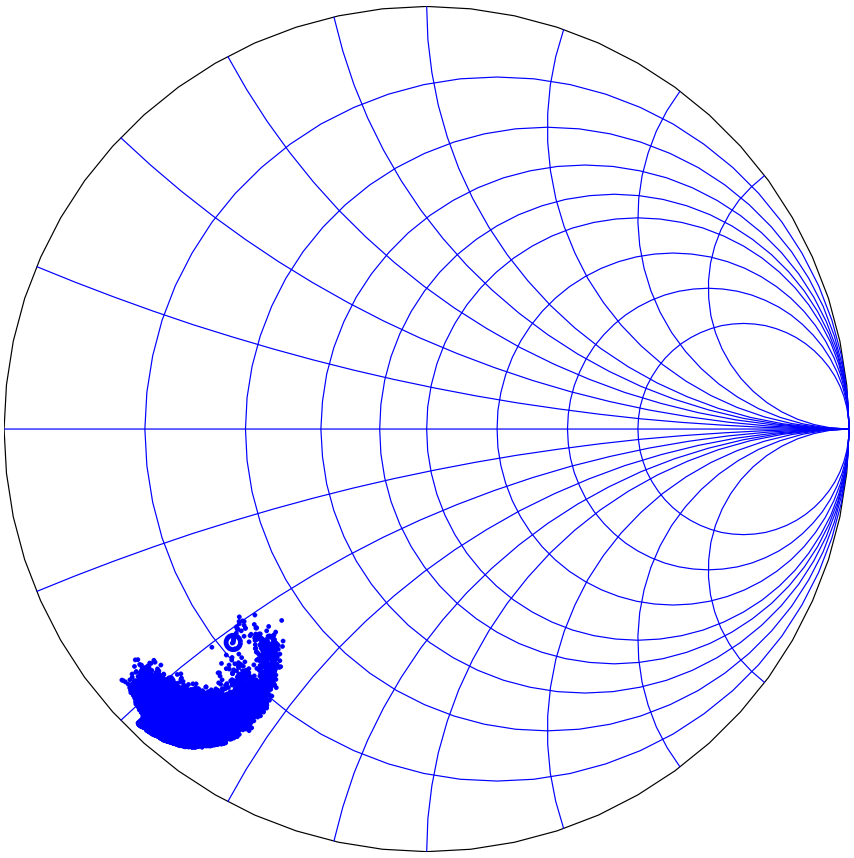

Figure 3.12: Impedances of 100,000 random states at 600 MHz

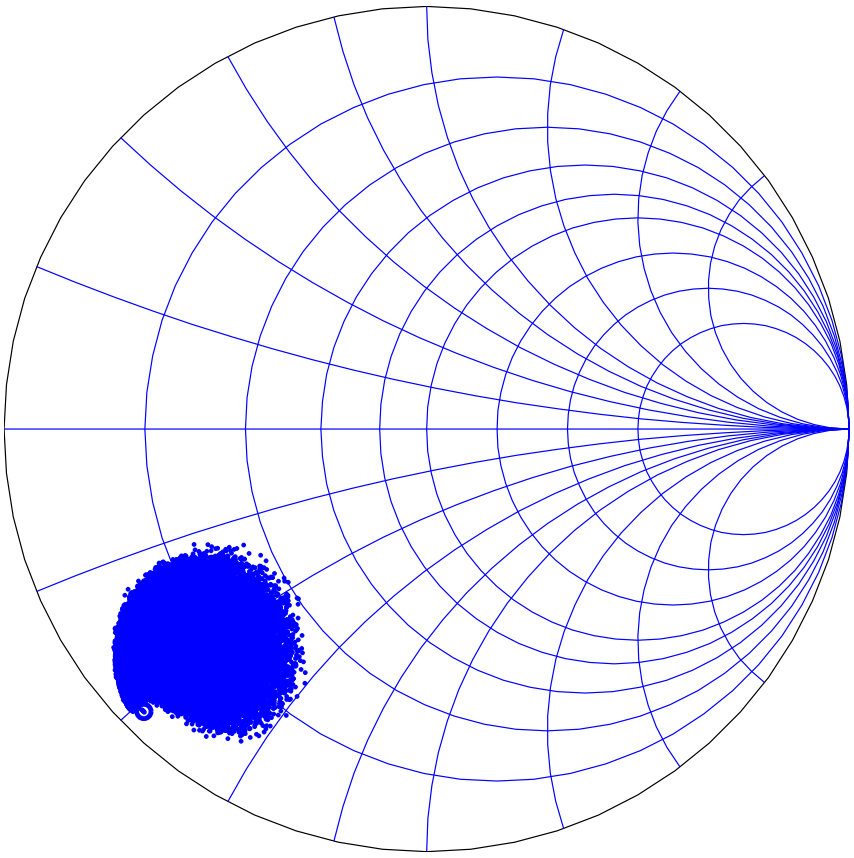

Figure 3.13: Impedances of 100,000 random states at 700 MHz

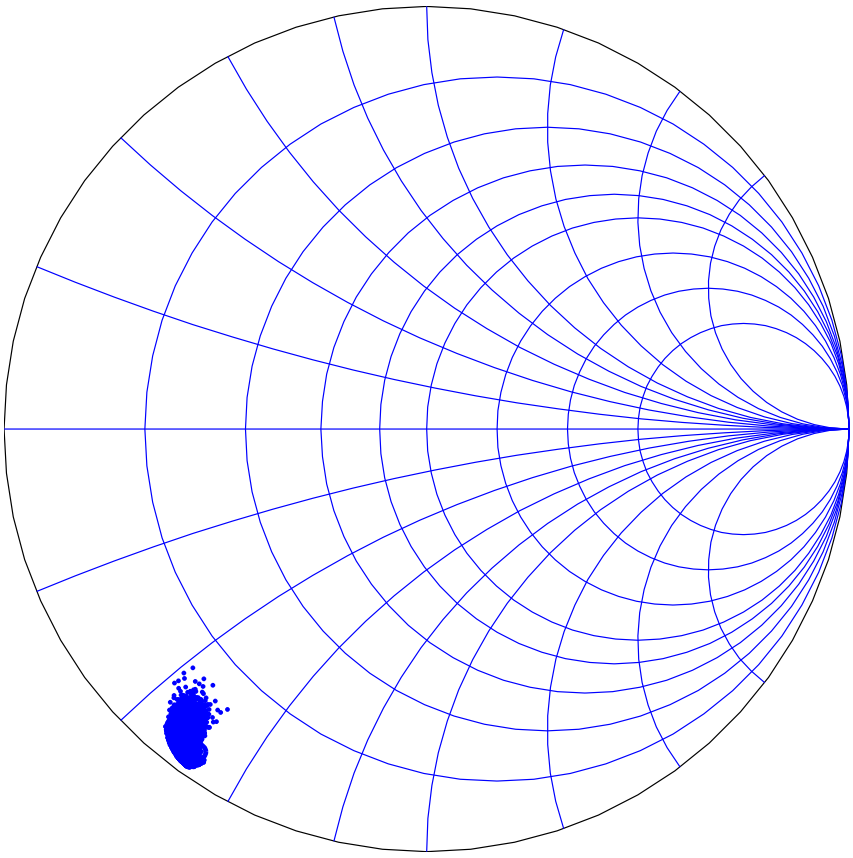

Figure 3.14: Impedances of 100,000 random states at 800 MHz

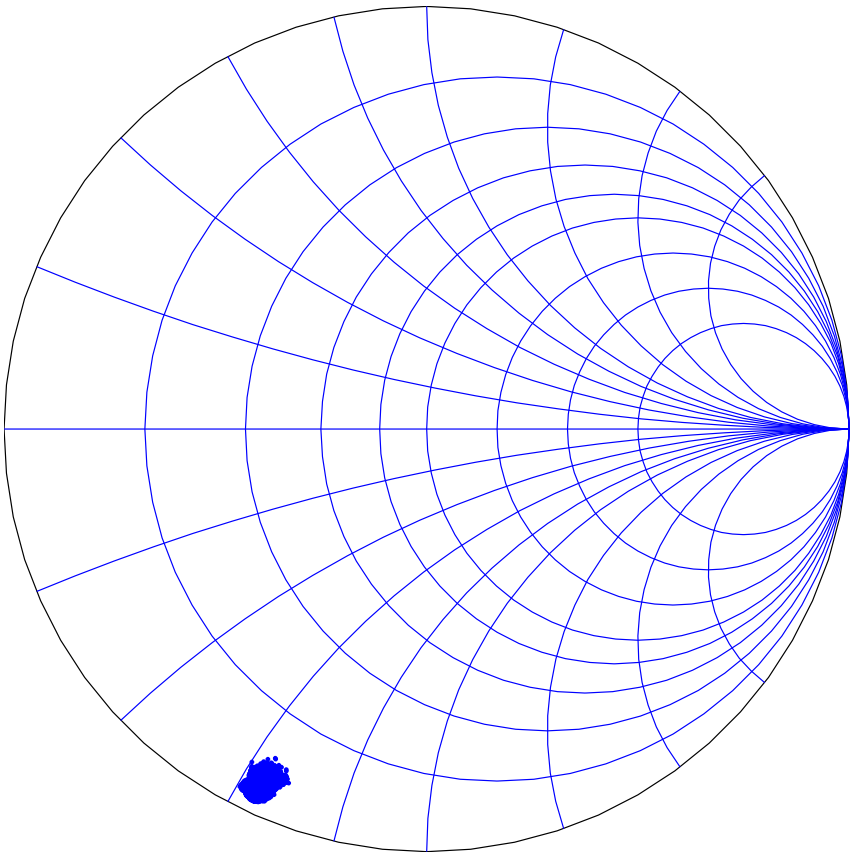

Figure 3.15: Impedances of 100,000 random states at 900 MHz

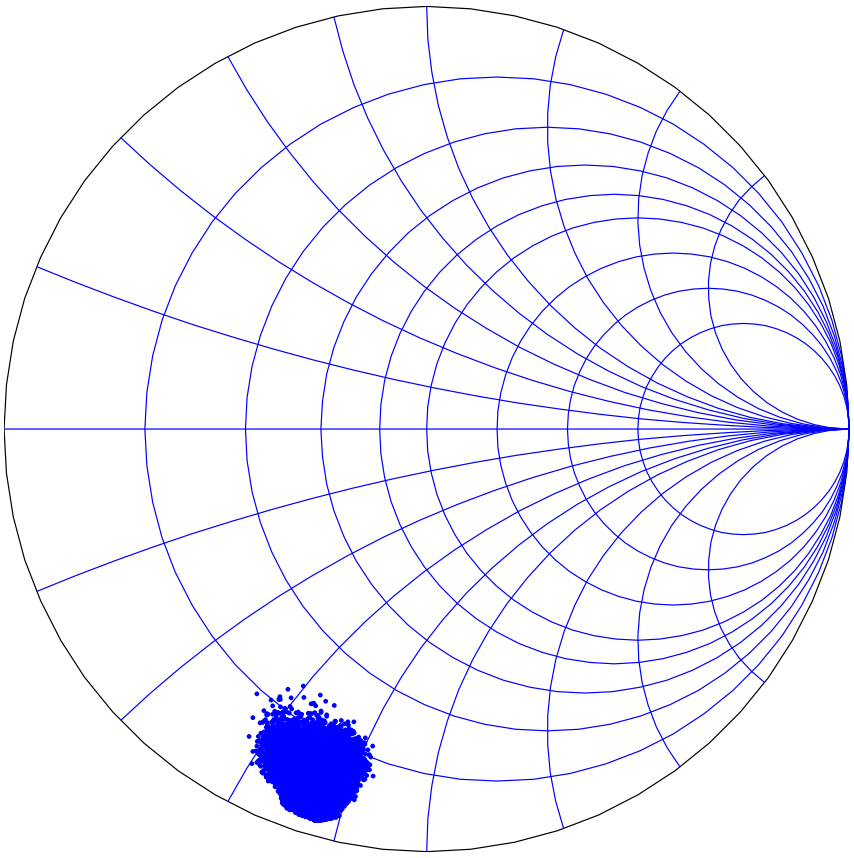

Figure 3.16: Impedances of 100,000 random states at 1 GHz

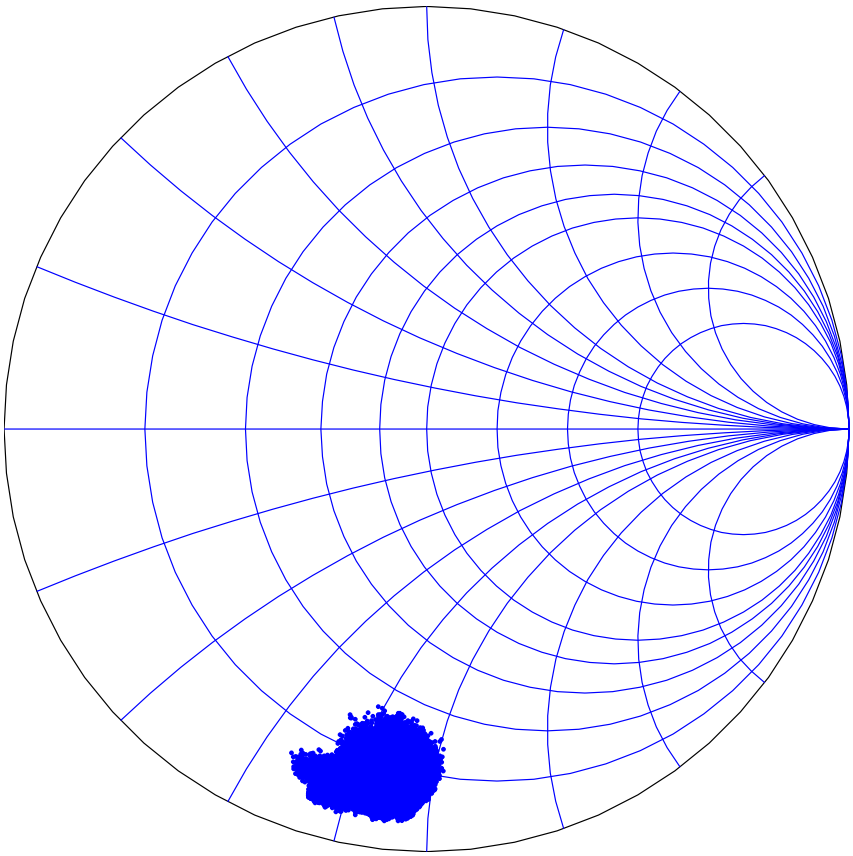

Figure 3.17: Impedances of 100,000 random states at 1.1 GHz

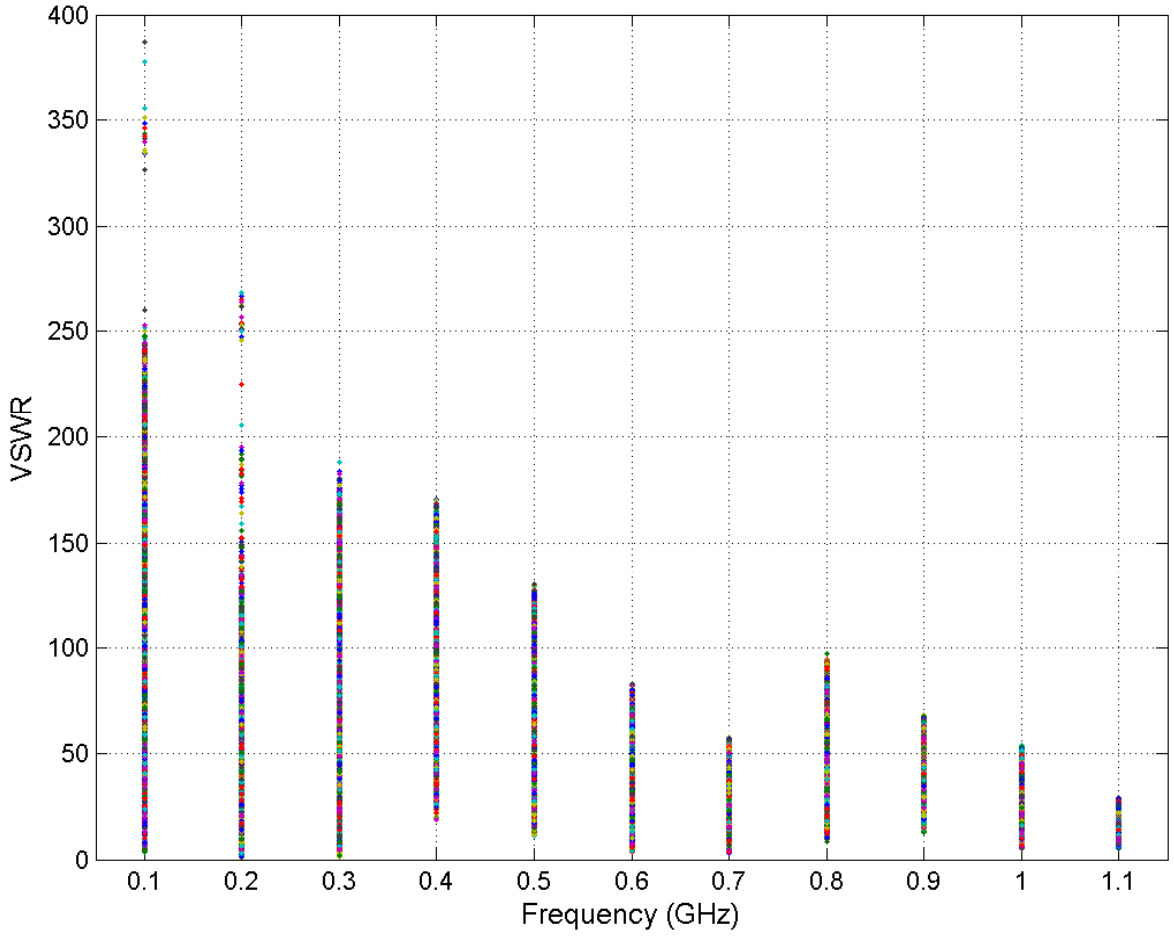

Figure 3.18: Random Search Measurements

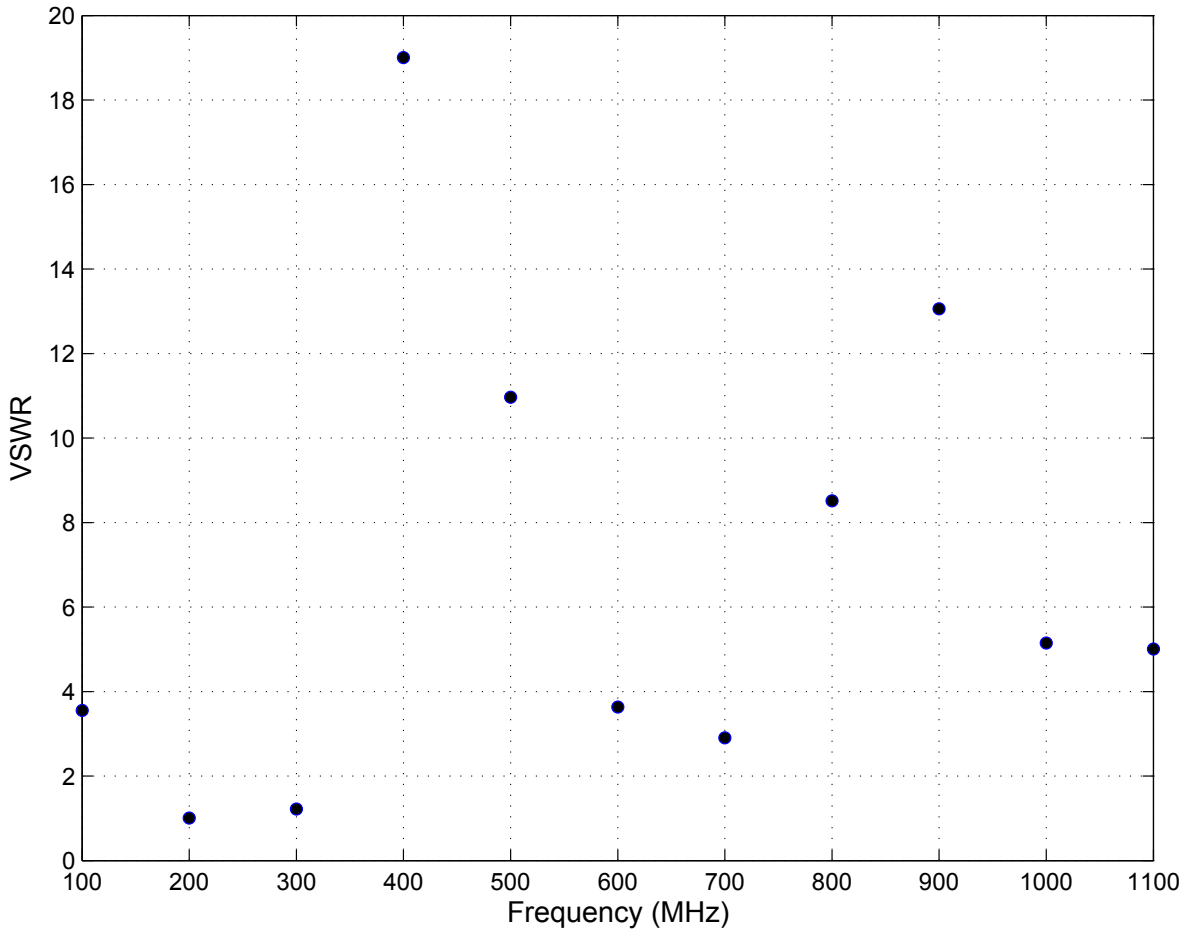

Figure 3.19: Random Search Measurements – minimum VSWR

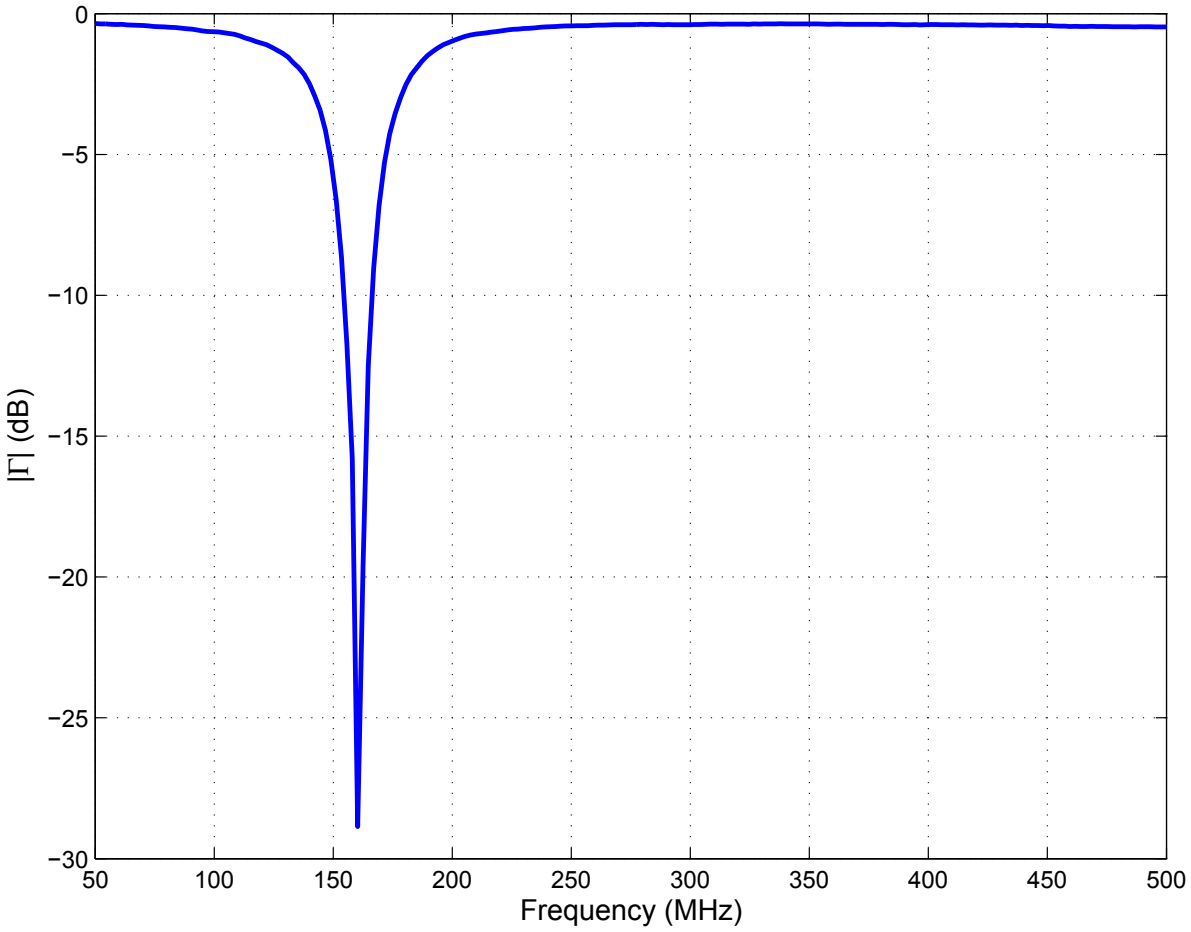

Figure 3.20: Magnitude of the reflection coefficient for head-worn antenna optimized at 160 MHz

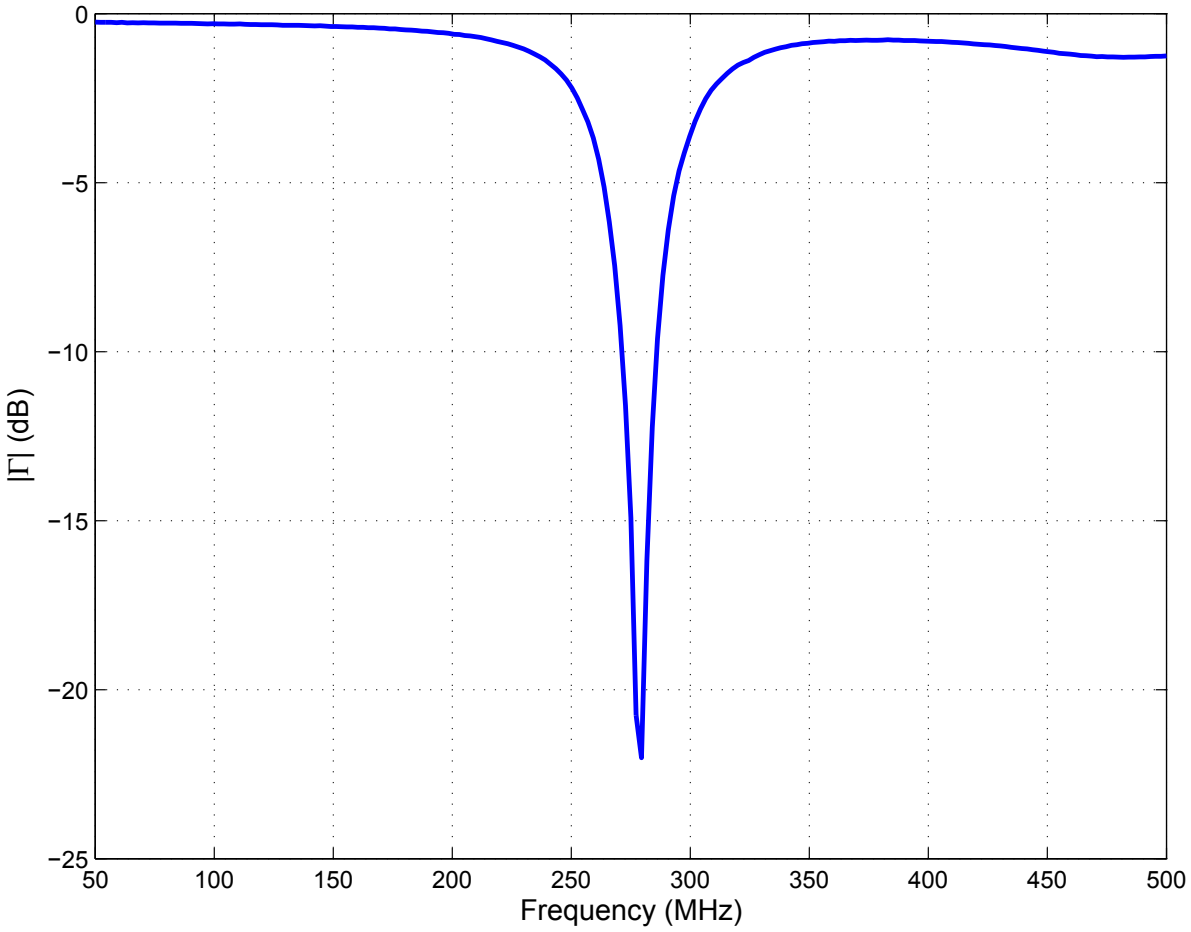

Figure 3.21: Magnitude of the reflection coefficient for head-worn antenna optimized at 280 MHz

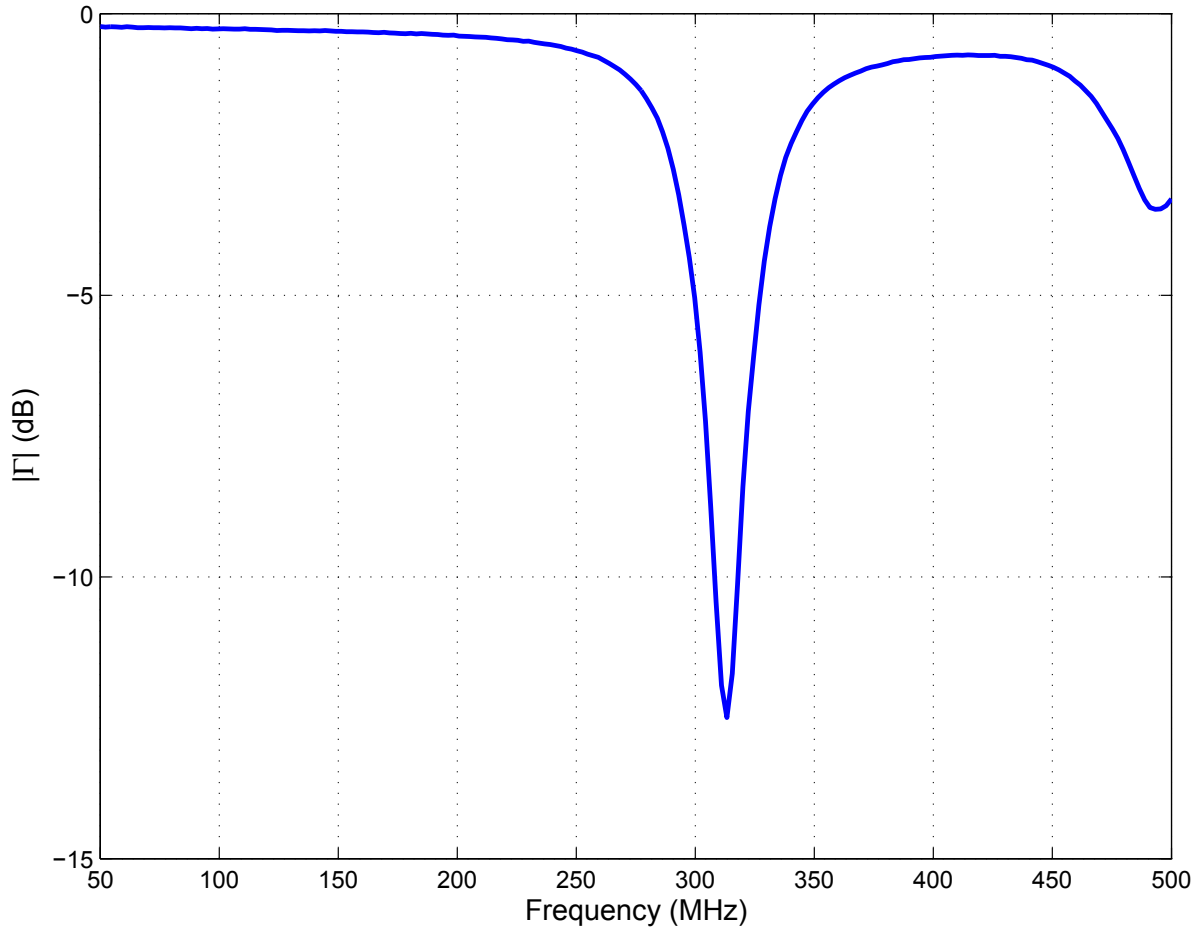

Figure 3.22: Magnitude of the reflection coefficient for head-worn antenna optimized at 320 MHz

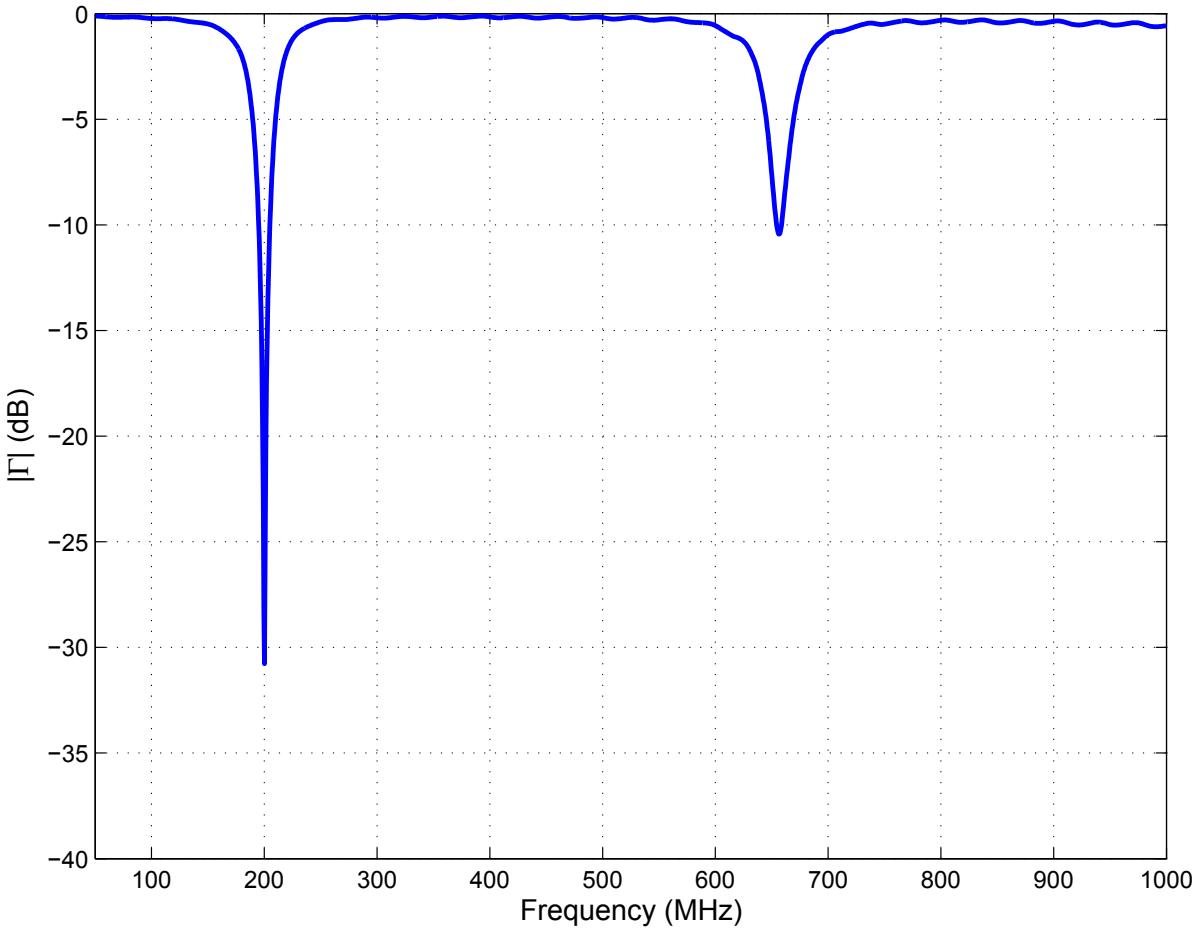

Figure 3.23: Magnitude of the reflection coefficient for head-worn antenna optimized at 200 MHz

Table 3.1: Random Search vs. GA

Frequency (MHz)	$VSWR_{random}$	$VSWR_{opt}$
200	1.0046	1.0590
300	1.2172	1.0470
400	19.003	5.0950
500	10.9669	7.5710
600	3.6329	3.9685
700	2.9058	1.9563
800	8.5115	7.6602
900	13.0562	13.7610
1000	5.1457	3.7966
1100	5.0073	4.3089

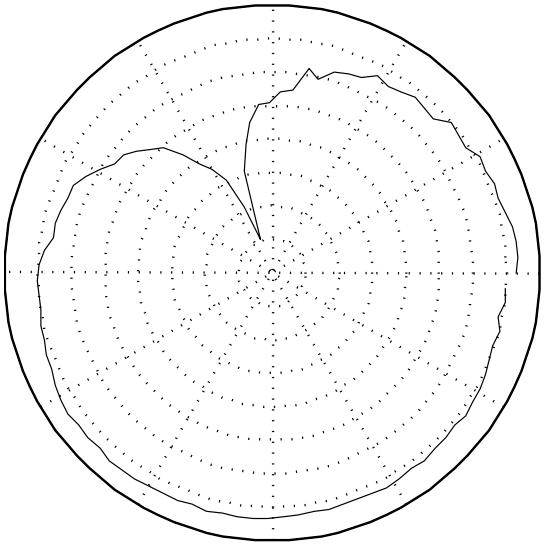

Figure 3.24: Pattern of best state at 200 MHz – Azimuthal plane

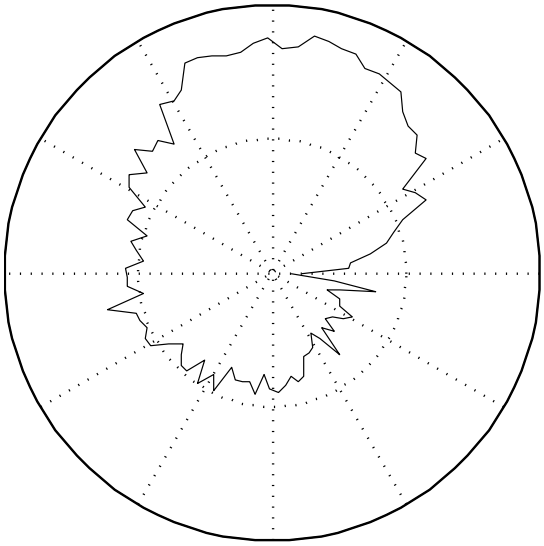

Figure 3.25: Pattern of best state at 200 MHz – Elevation plane

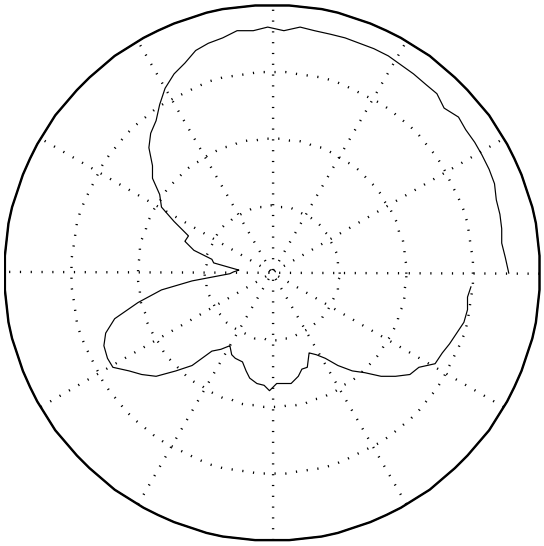

Figure 3.26: Pattern of best state at 280 MHz – Azimuthal plane

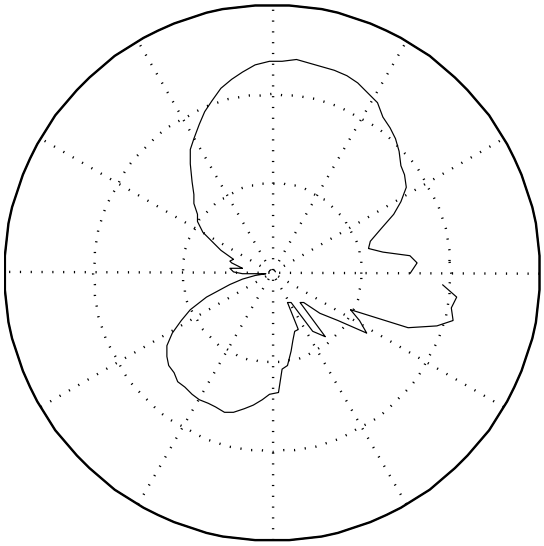

Figure 3.27: Pattern of best state at 280 MHz – Elevation plane

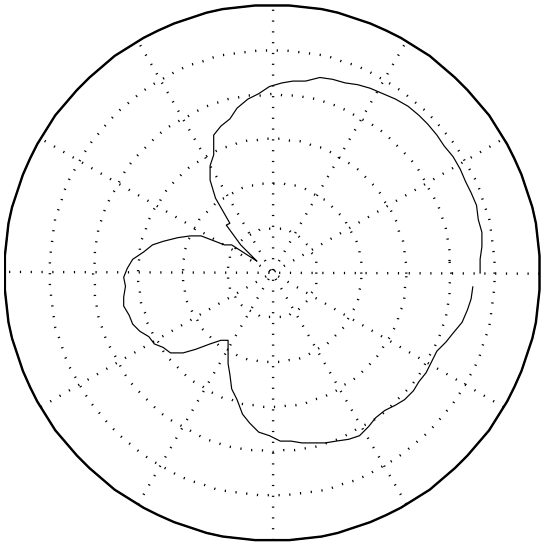

Figure 3.28: Pattern of best state at 320 MHz – Azimuthal plane

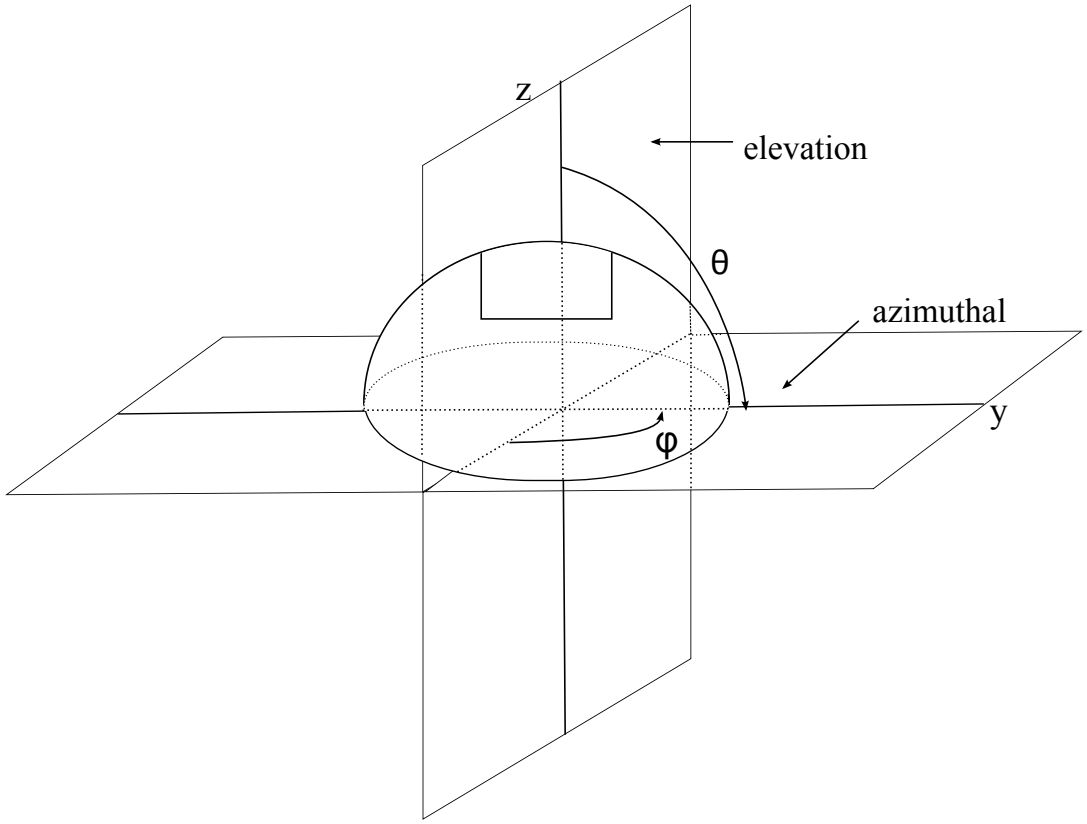

Figure 3.29: Figure illustrating pattern plane measurement designation

Chapter 4

Conclusions & Future Work

A self-structuring head-worn antenna is presented in this thesis. The first chapter serves as an introductory chapter, providing a description of recent work in the design of wearable antennas. It follows this by providing insight into the motivation behind the proposed head-worn antenna which is a union of the self structuring antenna idea and a curved patch antenna.

The second and third chapters detail simulations and experimental measurements carried out on the proposed head-worn antenna. The results obtained from the simulations in Chapter 2 show good return loss values that correspond to acceptable antenna performance at the desired frequencies. Hence, feasibility of the head-worn antenna over the frequency range (1 GHz – 2 GHz) was established before moving on to fabrication. Pattern results obtained from simulations show that adequate shielding is provided for a simulated human head model by the presence of the ground plane of the patch antenna . Additionally, the results point toward the possibility of multiple frequency operation for the head-worn antenna. As many as three distinct frequencies are resolved in some of the antenna configurations that are presented.

Experiments carried out on a fabricated prototype of the head-worn antenna are presented in the third chapter. All the necessary fabrication was done in-house. Initial experiments

were carried out in the form of random searches of $100,000$ antenna states at different frequencies. Targeted optimizations were run with a genetic algorithm at the same frequencies that the random search were run. At all but one of the frequencies, the genetic algorithm was able to find states with lower VSWR values in less looks. Additionally, measured pattern results were consistent with the expectation that radiation behind the ground plane would be minimal.

This work provided insight into the operation of the self-structuring antenna over a conformal surface. The results obtained are consistent with the established operation of the self-structuring antenna. Constraints imposed due to computational costs made it impossible for a detailed model of the human head to be used in the simulations. It is proposed that this be considered in future work with the self-structuring head-worn antenna. This work can lay the basis for the design and fabrication of more sophisticated body-borne antennas that incorporate the self-structuring antenna concept. Novel fabrics and polymers can be employed in the fabrication of such antennas to allow for greater flexibility.

Bibliography

Bibliography

[1] J.J.H. Wang, *"Broadband Omnidirectional Helmet Antennas"*, IEEE Antennas and Propagation Society International Symposium 2006, IEEE, pp.2129-2132, 9-14 July 2006

[2] J. Lebaric, Ah-Tuan Tan, *"Ultra-wideband Conformal Helmet Antenna"*, Microwave Conference, 2000 Asia-Pacific, pp.1477-1481, 2000

[3] Y. Rahmat-Samii, *"Wearable and Implantable Antennas in Body-Centric Communications"* Antennas and Propagation, 2007. EuCAP 2007, pp.1-5, 11-16 Nov. 2007

[4] C.M. Coleman, E.J. Rothwell, J.E. Ross, and L.L. Nagy, *"Self-Structuring Antennas"*, IEEE Antennas Propagat. Mag., pp. 11–23, June 2002.

[5] L.M. Greetis and E.J. Rothwell, *"A self-structuring patch antenna"*, APS (2008).

[6] FEKO,Suite5.0,EM Software and Systems-S.A. Ltd.,Stellenboch, South Africa. www.feko.info

[7] C.M. Coleman, E.J. Rothwell, and J.E. Ross, *"Investigation of simulated annealing, ant-colony optimization and genetic algorithms for self-structuring antennas"*, APS (2004).

[8] http://www.johnross.com/

[9] J.M. Johnson, V. Rahmat-Samii, *"Genetic algorithms in engineering electromagnetics"* Antennas and Propagation Magazine, IEEE , vol.39, no.4, pp.7-21, Aug 1997

[10] B. Perry et al, *"Effect of switch failure on the performance of a self-structuring antenna"*, APS (2002).

[11] B.T. Perry, C.M. Coleman, B.F Basch, E.J. Rothwell, J.E. Ross, and L. Nagy, *"Self-structuring antenna for television reception"*, (2001).

[12] C. Coleman, B. Perry, E. Rothwell, L. Kempel, J.E. Ross, and L. Nagy, *"A study of simple self-structuring antenna templates"*, (2002).

[13] S. Gabriel, R.W. Lau, C. Gabriel, *"The dielectric properties of biological tissues: III. Parametric models for the dielectric spectrum of tissues"* Phys Med Biol 41: 2271 - 2293. (1996).

[14] S. Gabriel, R.W. Lau, C. Gabriel, *"The dielectric properties of biological tissues: II. Measurements in the frequency range 10 Hz to 20 GHz"* Phys Med Biol 41: 2251 - 2269. (1996).

[15] S. Gabriel, R.W. Lau, C. Gabriel, *"The dielectric properties of biological tissues: I. Literature Survey"* Phys Med Biol 41: 2231 - 2249. (1996).

[16] K.S. Cole, R.H. Cole, *"Dispersion and absorption in dielectrics: I. Alternating current characteristics"* J Chem Phys 9: 341 - 351

[17] D.W. Davidson, R.H. Cole, *"Dielectric relaxation in glycerol, propylene, glycol and n-propanol"* J Chem Phys 19: 1484 - 1490.

[18] Balanis *"Antenna Theory: Analysis and Design"*

[19] http://www.fcc.gov/oet/rfsafety/dielectric.html

[20] D. Psychoudakis, C.C. Chen, J.L. Volakis, *"Optimizing wearahle UHF antennas for on-body operation"* Antennas and Propagation Society International Symposium, 2007 IEEE , pp. 4184-4187, 9-15 June 2007

[21] J.C.G. Matthews, G. Pettitt, *"Development of flexible, wearable antennas"* EuCAP 2009, 3rd European Conference on Antennas and Propagation, 2009, pp. 273-277, 23-27 March 2009

[22] Y. Rahmat-Samii, *"Wearable and Implantable Antennas in Body-Centric Communications"* Antennas and Propagation, 2007. EuCAP 2007, pp.1-5, 11-16 Nov. 2007

[23] L.M. Greetis and E.J. Rothwell, *"A self-structuring patch antenna"*, APS (2008).